Power spectrum analysis in supersonic/hypersonic turbulent boundary layers

Christian J. Lagares-Nieves[1]* and Guillermo Araya[1]†
[1]*HPC and Visualization Lab, Dept. of Mechanical Eng., University of Puerto Rico at Mayaguez, PR 00681, USA.*

Large databases of Direct Numerical Simulation (DNS) of spatially-developing turbulent boundary layers (SDTBL) are scrutinized. The major purpose is to evaluate compressibility effects on power spectra of velocity fluctuations at the supersonic (M_∞ = 2.86) and hypersonic (M_∞ = 5.0) regime. An incompressible SDTBL is also examined. In all cases, the Reynolds numbers are sufficiently high in order to obtain a noticeable separation of turbulent scales. Adiabatic wall conditions are assumed for the compressible cases; whereas, an isothermal wall condition is prescribed for the incompressible flow (temperature regarded as a passive scalar) over Zero-Pressure Gradient (ZPG) flat plates. Turbulent inflow information is generated via a dynamic rescaling-recycling approach [1], which avoids the use of empirical correlations in the computation of inlet turbulent scales. This approach has been recently extended to compressible wall-bounded flows [2]. In general and based on power spectrum analysis, we observe a reduction in the dimensions of the coherent structures as Mach number increases. Further, as the Mach number grows, the structures become narrower and their downstream influence is notably diminished. The inner peak of the streamwise component of the Reynolds normal stresses, $(u'u')^+$, coincides with the major peak in the pre-multiplied spectra at roughly $y^+ = 10 - 15$. A less energetic but obvious secondary peak is found in the region $y^+ \approx$ 100-150 of the pre-multiplied spectra of u'. Further, the proposed inflow condition generation method proposed by Araya *et al.* [1, 2] was demonstrated to be highly robust with a minimal development region (in the order of $2.5\delta's$ at most) and an energy spectra resembling that of a fully developed flow. Interestingly, the outflow condition selection was found to have a more detrimental impact on the quality of the energy spectra.

I. Nomenclature

R_{δ_2}	=	Momentum thickness Reynolds number
M_∞	=	Freestream Mach number
U_∞	=	Freestream velocity
U^+_{VD}	=	Van Driest transform velocity in wall units
T_∞	=	Freestream temperature
T_r	=	Recovery temperature
T_w	=	Wall temperature
ν_w	=	Wall kinematic viscosity
u_τ	=	Friction velocity
P	=	Mean Pressure
T	=	Mean Temperature
k	=	Thermal conductivity
c_p	=	Specific heat at constant pressure
N_t	=	Number of Temporal Samples
N_s	=	Number of Additional Smoothing Samples
N_x	=	Number of Nodes Along the Streamwise Direction
N_y	=	Number of Nodes Along the Wall Normal Direction
N_z	=	Number of Nodes Along the Spanwise Direction

*PhD Research Assistant & Doctoral Candidate, Department of Mechanical Engineering, 259 Alfonso Valdez Blvd., Mayaguez, PR, 00680, and Student Member

†Associate Professor, Department of Mechanical Engineering, 259 Alfonso Valdez Blvd., Mayaguez, PR, 00680. AIAA Associate Fellow

μ	=	Molecular Viscosity
ρ	=	Density
δ	=	Boundary layer thickness
τ	=	Shear stress
Subscript	=	
inl	=	inlet
rec	=	recycle
$_{rms}$	=	Root-Mean Squared
$'$	=	Superscript denotes fluctuating components
∞	=	Subscript denotes freestream quantities

II. Introduction

Unsteady spatially-developing turbulent boundary layers (SDTBL) are the rule rather than the exception in a wide range of disciplines and engineering applications, showing non-homogeneous conditions along the flow direction. Furthermore, compressible SDTBL's are ubiquitous and play a key role in the transport phenomena of high speed flight conditions with applications ranging from space planes, to future commercial planes, military technologies, space exploration technologies, among many others. A key aspect of the understanding and modelling of SDTBLs is the distribution of energy among the length and time scales. Also, to reduce the cost of high spatial/temporal resolution Direct Numerical Simulation (DNS) and to circumvent starting the simulations from the laminar stage (as well as to spot high Reynolds numbers), physically accurate turbulent inflow conditions must be prescribed with a realistic energy spectrum. Additionally, investigation performed during the past decades has conclusively proven the presence of organized motions in turbulent boundary layers, so called coherent structures (CS). A coherent structure may be defined as a region or parcel of fluid where the flow fluctuations are highly correlated among them. These structures can be considered the core of turbulent boundary layers, and significant effort has been invested to describe their development. Further, these large scales of motion follow highly complex, non-linear dynamics where the level of coherence should be quantifiable [3]. Identifying these very-large scales of motion (VLSMs) can be done in a myriad of possible ways depending on how the problem is stated. One such avenue is to employ energy spectra [4] and two-point correlations [5] which can be efficiently computed with low memory requirements via high-performance inner products [6] or a more memory-intensive (but higher fidelity) FFT-based convolution [7, 8].

The nature and existence of these organized structures was explored early by Spina and Smits[9]. Rempfer and Fasel [10] also explored the nature of these coherent structures in a volumetric space. They employ proper orthogonal decomposition which translates the problem of computing these structures into an Eigenvalue problem. Closely related work by Aubry *et al.* [11], further reinforced the existence of a link between low-dimensional chaotic dynamics and properties of realistic turbulence. Smits *et al.* [12] also explored the structure of the turbulent boundary layer with a special focus on comparing the subsonic and supersonic SDTBLs. They concluded that albeit many similarities (especially along the spanwise direction) are indeed present there exists drastic differences such as variations in length scales. Work by Ringuette *et al.*[13], explored volumetric coherent structures for a Mach 3 boundary layer and contrasted it with a subsonic boundary layer. Although they used several methods for visualizing the above mentioned VLSMs, and the two-point correlation technique was among the selected methodologies. Later work by Elsinga *et al.*[14] sought to explore the organization of vortex for high Reynolds supersonic SDTBLs. They also employed the autocorrelation function and provided conclusions related to the periodic nature of these coherent structures, their lengths and inclinations. Although a large portion of work previously outlined has been computational in nature, work by He *et al.* [15] visualized these coherent structures for an experimental supersonic boundary layer over a flat plate. Another seminal contribution by Sillero *et al.* [16], which was further elaborated by Jimenez [3], explored in detail the 3D nature of turbulent coherent structures by the two-point correlation in incompressible flow. Dharmarathne *et al.* provided a more applied view of the impact of turbulent coherent structures in passive scalar transport [17] via DNS of incompressible channel flows. More recently, TPC's have been employed to assess wall-temperature effects at hypersonic conditions [18] at low Reynolds numbers.

As previously mentioned, the assessment of VLSMs can also be achieved by exploring the energy spectra. The work by Hutchins and Marusic studied the influence of VLSMs in near-wall turbulence through the exploration of the energy content at different scales [4]. Another work by Hutchins and Marusic [19] explored the use of the pre-multiplied energy spectra, among other techniques, for the identification of coherent structures in the log region of a turbulent boundary layer. Álamo *et al.* explored the intensity and contributions of Reynolds shear stresses by studying the pre-multiplied

uv-cospectra [20] which highlights the versatility of the approach. This approach has also been used to discriminate and assess the effects of freestream turbulence from structures within the boundary layer by Sharp *et al.* [21]. Sciacovelli *et al.* also explored near wall structures of supersonic boundary layers for dense gases in a channel flow via DNS by using multiple techniques including pre-multiplied spectra. More recently, Huang *et al.* leveraged pre-multiplied pressure energy spectra to identify peak intensity in the near-wall and freestream at hypersonic conditions [22].
In the present work, we conduct a study of the compressibility effects in the normalized and pre-multiplied energy spectra at both supersonic and hypersonic conditions. Further, we also assess the strength of the turbulent inflow condition generation method proposed by Araya *et al.* [1] [2]. This latter objective will be assessed by studying the distribution of the energy spectrum near the inlet and comparing it with the energy spectrum halfway through the computational domain. Also, we compare the characterization of coherent structures obtained by pre-multiplied spectra with full domain two-point correlations.

III. Governing Equations

Assuming continuum mechanics and neglecting non-equilibrium effects yields the usual system of non-linear partial differential equations known as the compressible Navier-Stokes equations [23]. Conservation of mass becomes non-trivial for compressible flow with strong pressure gradients, compression and expansion waves where density varies abruptly. The classical conservation equations are presented in eqns. 1, 2 and 3.

$$\frac{\partial \rho}{\partial t} + \frac{\partial}{\partial x_j}\left(\rho u_j\right) = 0 \tag{1}$$

$$\frac{\partial \rho u_i}{\partial t} + \frac{\partial}{\partial x_j}\left(\rho u_i u_j + p\delta_{ij} - \sigma_{ij}\right) = 0 \tag{2}$$

$$\frac{\partial \rho e}{\partial t} + \frac{\partial}{\partial x_j}\left((\rho e)u_j - u_i\sigma_{ij} + q_j\right) = 0 \tag{3}$$

where ρ is the density; u_i is the velocity in the i direction; p is the pressure; σ_{ij} is the stress tensor which we model as a linear stress-strain relationship,

$$\sigma_{ij} = 2\mu S_{ij} - \frac{2}{3}\mu\delta_{ij}S_k k \tag{4}$$

where $S_{ij} = \frac{1}{2}\left(\frac{\partial u_i}{\partial x_j} + \frac{\partial u_j}{\partial x_i}\right)$ is the strain rate tensor, μ is the kinematic viscosity; and q_i is the hear flux due to thermal gradients in the i direction and is modelled in the present work by Fourier's law, $q_i = \kappa\frac{\partial T}{\partial x_i}$ where κ is the thermal conductivity; e is total energy per unit mass which we assume to follow:

$$e = c_v T + \frac{1}{2}u_i u_j \tag{5}$$

where c_v is the specific heat at constant volume. Finally, we also assume the fluid viscosity to vary following a Power Law (see Equation 6).

$$\mu = \mu_\infty\left(\frac{T}{T_\infty}\right)^{0.76} \tag{6}$$

The equations are all presented in their strong form whereas the weak form is used in the finite element solver. The present work leverages the PHASTA flow solver [24]. The finite element scheme is based on the streamline upwind Petrov-Galerkin (SUPG) finite element discretization in space with a second order accuracy [25, 26]. The non-linear system of equations are solved using an iterative Krylov solver in space while being fully implicit in time (2^{nd} order accurate). Further details regarding the finite element method employed are beyond the scope of this work, readers are referred to [27].

IV. Numerical Details

A. Turbulent Inflow Conditions, DNS Details and Validation

Modeling aspects of the physics of SDTBL via DNS must account for the following aspects: i) the mesh resolution must be adequate in order to capture the smallest turbulence momentum/thermal scales (Kolmogorov and Batchelor

scales), ii) the computational domain should be large enough to contain even the largest scale motions (LSM) or "superstructures" (Hutchins & Marusic [19] [4]), iii) as previously articulated, realistic time-dependent inflow turbulent fluctuations must be injected, Araya *et al.*, [1] [2], and, iv) connected to the previous point, the turbulent inflow fluctuations must possess the proper power spectrum to minimize the "inlet developing section" (ideally, this section should be in the order of 2-3 δ_{inl}'s). In a nutshell; first, adequate turbulent inlet conditions permit simulating even larger Reynolds numbers (i.e., large scale systems) since resolving the laminar-transition stage is not required anymore; and, second, the streamwise domain length is optimized insomuch as the "non-physical" developing section is curtailed. In the present article, the inlet generation methodology proposed by Araya *et al.* [1] is used, called Dynamic Multiscale Approach (DMA), which was recently extended to compressible SDTBL in [2] and [28]. It is a modified version of the rescaling-recycling technique by Lund *et al.* [29]. Extensions to compressible boundary layers have also been proposed by Urbin & Knight [30], Stolz & Adams [31] and Xu & Martin [32]. The present inflow generation technique avoids using empirical correlations to connect the inlet friction velocity to the recycle friction velocity, as will be described later in the manuscript. A schematic of the hypersonic computational domain is shown in fig. 1 where iso-contours of instantaneous density can be observed. The fundamental idea of the rescaling-recycling method is to extract the flow solution (mean and fluctuating components of the velocity, thermal and pressure fields for compressible flows) from a downstream plane (called "recycle") and after performing a transformation by means of scaling functions, the transformed profiles are re-injected at the inlet plane, as seen in figure 1. *Actually, it has been observed that just fixing the mean pressure at the inlet plane produced more stable and accurate numerical cases than adding pressure fluctuations*. According to [33] and [30], "the static pressure can be assumed constant at the inlet plane since the pressure fluctuations are small compared to the static temperature fluctuations". Instantaneous density profiles (mean plus fluctuations) are indirectly imposed due to the equation of state for a perfect gas. This can be visually verified from fig. 1. The principal idea of implementing scaling laws to the flow solution is to convert the streamwise in-homogeneity of the flow into quasi-homogeneous conditions. The Reynolds decomposition is implemented for instantaneous parameters, i.e. a time-averaged plus a fluctuating component:

$$u_i(\mathbf{x}, t) = U_i(x, y) + u_i'(\mathbf{x}, t) \tag{7}$$

$$t(\mathbf{x}, t) = T(x, y) + t'(\mathbf{x}, t) \tag{8}$$

The SDTBL is divided into inner and outer zones, where different scaling laws are applied [1] in a multiscale fashion. A blending or weight function is used to create composite instantaneous flow profiles for smoothly merging inner and outer zone contributions. The projection of flow parameters from the recycle plane to the inlet is performed along constant values of y^+ (inner region) and y/δ (outer region). Figure 1 depicts the schematic of the computational domain in the hypersonic regime at high Reynolds numbers. In the re-scaling process of the flow parameters [1], the ratio of the inlet friction velocity to the recycle friction velocity (i.e., $\lambda = u_{\tau,inl}/u_{\tau,rec}$) is required. The friction velocity is defined as $u_\tau = \sqrt{\tau_w/\rho}$, where τ_w is the wall shear stress and ρ is the fluid density. Since the inlet boundary layer thickness must be prescribed according to the predicted inlet Reynolds number, prescribing also the inlet friction velocity would be redundant. To solve this problem, Lund *et al.* [29], Urbin & Knight [30] and Stolz & Adams [31] employed the well-known one-eighth power law that connects the friction velocity to the momentum thickness in zero-pressure gradient flows; thus, $u_{\tau,inl}/u_{\tau,rec} = (\delta_{2,inl}/\delta_{2,rec})^{-1/8}$. The empirical power (-1/8) might be strongly affected by the Reynolds number dependency plus some compressibility effects; therefore, we "dynamically" calculated this power exponent, $\gamma_{\delta 2}$, by relating the mean flow solution from a new plane (so-called the "Test" plane, as seen in figure 1) to the solution from the recycle plane as follows:

$$\gamma_{\delta 2} = \frac{ln(u_{\tau,test}/u_{\tau,rec})}{ln(\delta_{2,test}/\delta_{2,rec})}. \tag{9}$$

Figure 2 (a) exhibits a representative time series of the local computed friction velocities at the Inlet, Test and Recycle planes in the hypersonic flat plate at high Reynolds numbers. Notice that friction velocities have been normalized by the local freestream velocity. In particular, this hypersonic case ($M_\infty = 5$) was initialized via a previously run supersonic DNS case ($M_\infty = 2.5$), as in [2], to shorten the transient. A similar strategy was carried out for the supersonic case ($M_\infty = 2.86$) in this study. It is observed a clear transient stage ($t^+ \approx 14,000$) where friction velocities fluctuate wildly. Beyond $t^+ \approx 14,000$, all friction velocities tend asymptotically towards specific values. Flow statistics was sampled in the last 1,400 inner time. Friction velocities at the test and recycle plane (as well as momentum thicknesses) are computed "on the fly" based on the time-averaged parameters from the flow solution. Once the exponent $\gamma_{\delta 2}$ is obtained from Eq. 9 based on test and recycle plane statistics, the values of $u_{\tau,inl}$ and λ can be dynamically computed. The

asymptotic value of λ ($= u_{\tau,inl}/u_{\tau,rec}$) was approximately 1.014 in the statistically steady stage. Figure 2 (b) exhibits the time variation of the boundary layer thickness at the different reference planes in wall units, δ^+, representing the von Karman or friction Reynolds number. It seems that the hypersonic flow depicts a moderate temporal transient at the boundary layer edge. This hypersonic DNS case possesses δ^+ values around 1,000 (and, similarly, the rest of the DNS cases presented in this manuscript) with a defined separation of turbulent scales, as is shown and discussed in the manuscript.

The present DNS cases at high Reynolds numbers are run by using a highly accurate, very efficient, and highly scalable CFD solver called PHASTA. The flow solver PHASTA is an open-source, parallel, hierarchic (2^{nd} to 5^{th} order accurate), adaptive, stabilized (finite-element) transient analysis tool for the solution of compressible [27] or incompressible flows [25]. PHASTA has been extensively validated in a suite of DNS under different external conditions [18, 34, 35].

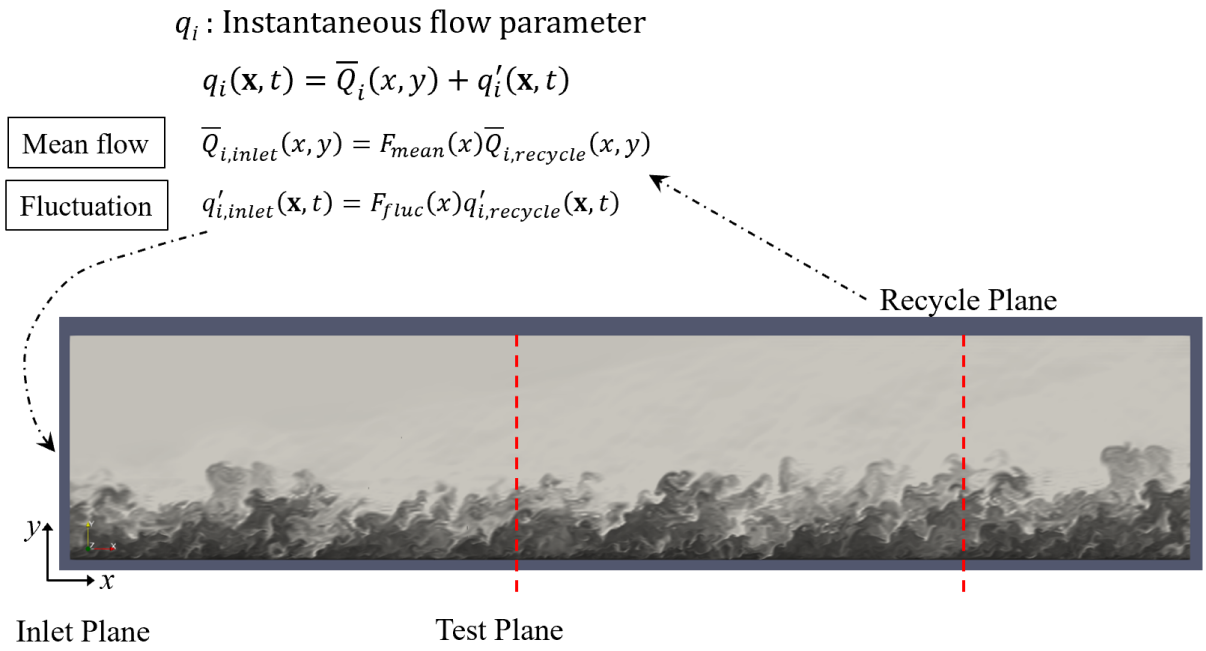

Fig. 1 Boundary layer schematic for the hypersonic case. Contours of instantaneous density.

Boundary Conditions: At the wall, the classical no-slip condition is imposed for all velocity components. Adiabatic wall conditions were applied for both compressible cases. For the supersonic flow case at Mach 2.86, the ratio T_w/T_∞ is 2.74 (in fact, quasi-adiabatic), where T_w is the wall temperature and T_∞ is the freestream temperature. While the T_w/T_∞ ratio is 5.45 for M_∞ equals to 5. In the incompressible case, temperature is regarded as a passive scalar with isothermal wall condition. In all cases the Prandtl number is 0.72. The lateral boundary conditions are handled via periodicity; whereas, freestream values are prescribed on the top surface.

Table 1 summarizes the characteristics of the analyzed two cases: the incompressible case ($M_\infty = 0$) and compressible cases ($M_\infty = 2.86$ and 5). The Reynolds number range, computational domain dimensions in terms of the inlet boundary layer thickness δ_{inl} (where L_x, L_y and L_z represent the streamwise, wall-normal and spanwise domain length, respectively) and mesh resolution in wall units (Δx^+, Δy^+_{min}, Δy^+_{max}, Δz^+) are also given. The DNS cases have the following grid point numbers: $990 \times 250 \times 210$ (roughly a 52-million point mesh). The cases were run in 1200 processors at the Onyx supercomputer (ERDC, DoD).
Figure 3 (a) shows the streamwise development of the skin friction coefficient of present DNS supersonic data at Mach 2.86. In addition, C_f values at Mach 2.5 are included from DNS of Araya et al. [2]. It is worth noting the excellent agreement of present DNS with experiments at similar Reynolds and Mach numbers from Stalmach [36]. Furthermore, DNS and experimental data from [37, 38] and [39], respectively, are also included at supersonic Mach numbers between 2 and 3. Figure 3 (b) depicts the streamwise development of the compressible momentum tickness Reynolds number,

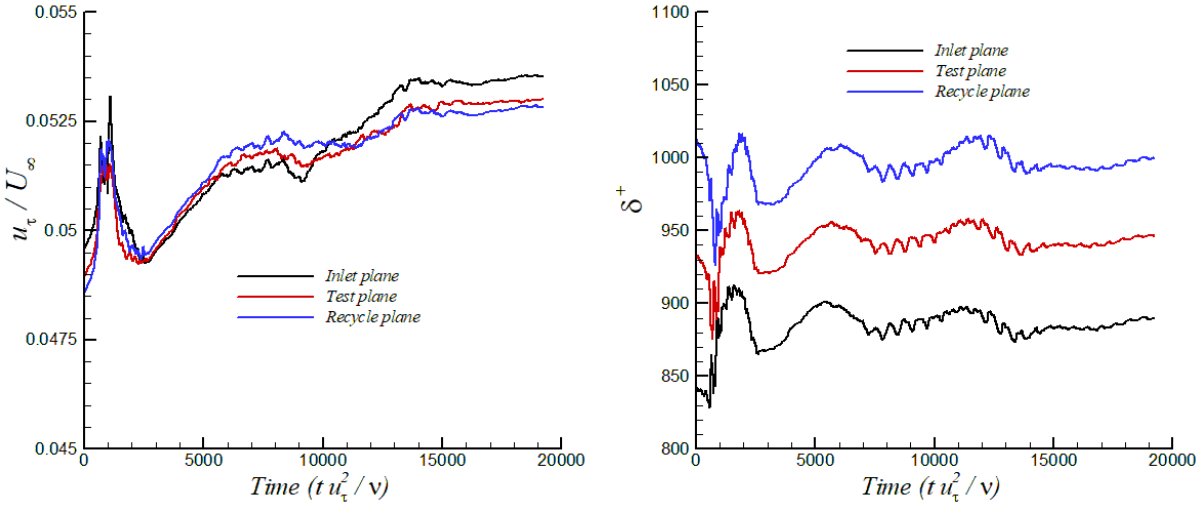

(a) (b)

Fig. 2 (a) Time-series of the friction velocity normalized by the local freestream velocity and (b) the local boundary layer thickness in wall units at the Inlet, Test and Recycle planes, respectively, for hypersonic flow with adiabatic wall condition.

$Re_{\delta 2}$ at $M_\infty = 2.86$. Clearly, the inlet developing section expands for just 2.5-δ_{inl}, indicating the good performance of the turbulent inflow generation method employed.

Figure 4 (a) shows the mean streamwise velocity normalized by the freestream velocity U_∞ at $M_\infty = 2.86$. A very good agreement is observed with experimental values by [40] and [41] at similar Mach numbers but at significantly higher Reynolds numbers. Some scattering on experimental data by [41] is observed. In addition, DNS data by Bernardini and Pirozzoli [38] is also included at a lower Reynolds number. The streamwise component of the normal Reynolds stresses u'^2, normalized by U_∞^2, are depicted by fig. 4 (b) in outer units. Present DNS agrees quite well with experiments by [40], particularly in the outer part of the boundary layer, i.e. for $y/\delta > 0.2$. The Reynolds number effect on peak values of the streamwise component of the Reynolds normal stresses can be defined as a displacement towards the near wall region as the former increases (see present DNS at $Re_{\delta 2} = 3528$ vs. [38] at $Re_{\delta 2} = 1815.7$). Furthermore, the streamwise and wall-normal components of the turbulence intensities are exhibited in fig. 4 (c) and normalized by the freestream velocity, U_∞. Major discrepancies with experiments of [41] are observed in the inner region for v'_{rms}, which may be attributed to some Reynolds number dependency; however, further analysis must be performed. Again, peaks of u'_{rms} and v'_{rms} are shifted towards the wall in our DNS case (at slightly larger Reynolds numbers) as compared to DNS by Bernardini and Pirozzoli [38]. The quality of the generated turbulent data at Mach 5 has been assessed, as well. Figure 5 (a) shows the mean streamwise velocity in outer units. Clearly, there is a very good agreement with experiments by Tichenor [42] in adiabatic flat plates at a freestream Mach number of 5. It is worth highlighting the effect of the Reynolds number in the inner region of the boundary layer (i.e., for $y/\delta < 0.1$): the profiles move toward the wall region as the Reynolds number increases. Notice DNS data from Duan et al. [43] and experiments by Neeb et al. [44] at much lower Reynolds numbers and Mach numbers around 5. Figure 5 (b) shows the mean streamwise velocity by means of the van Driest transformation. Overall, a very good agreement can be observed between our DNS with experiments by Mabey and Sawyer [45] at $M_\infty = 2.49$, in the log and wake region. Additionally, three different logarithmic laws, as used in [31], have been included. For high values of $Re_{\delta 2}$, the log region extends significantly (about 300 wall units in length). Obviously, the log region tends to "shrink" as the Reynolds number decreases, as seen in DNS data by [43] at $M_\infty = 5$. It seems our predicted values of U^+_{VD} are slightly better represented by the logarithmic function $1/0.41 ln(y^+) + 5$ as proposed by White [46] by the end of the log region (and beginning of the wake region). On the other hand, the log law as proposed by [47] (with a κ value of 0.38 and an integration constant, C, of 4.1) exhibits an excellent match with our DNS results in the buffer region (i.e., around $y^+ \approx 30$).

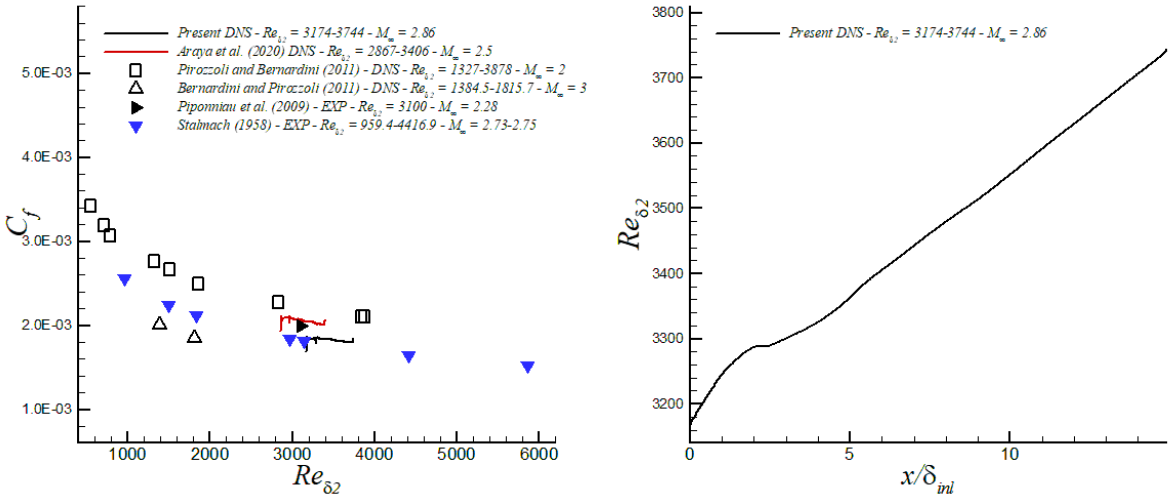

(a) (b)

Fig. 3 (a) Skin friction coefficient and (b) momentum thickness Reynolds number at M_∞ = 2.86.

Table 1 DNS Cases.

Case	**Flow fields**	M_∞	T_w/T_∞	$Re_{\delta 2}$	δ^+	$L_x \times L_y \times L_z$	Δx^+,$\Delta y^+_{min}/\Delta y^+_{max}$, Δz^+
Incompressible	2001	0	0	2000-2400	752-928	$16\delta_{inl} \times 3\delta_{inl} \times 3\delta_{inl}$	11.5, 0.4/10, 10
Supersonic	1001	2.86	2.74	3174-3744	847-995	$14.9\delta_{inl} \times 3\delta_{inl} \times 3\delta_{inl}$	12.7, 0.4/11, 12
Hypersonic	1001	5	5.45	4358-5050	899-1080	$15.2\delta_{inl} \times 3\delta_{inl} \times 3\delta_{inl}$	12, 0.4/12, 11

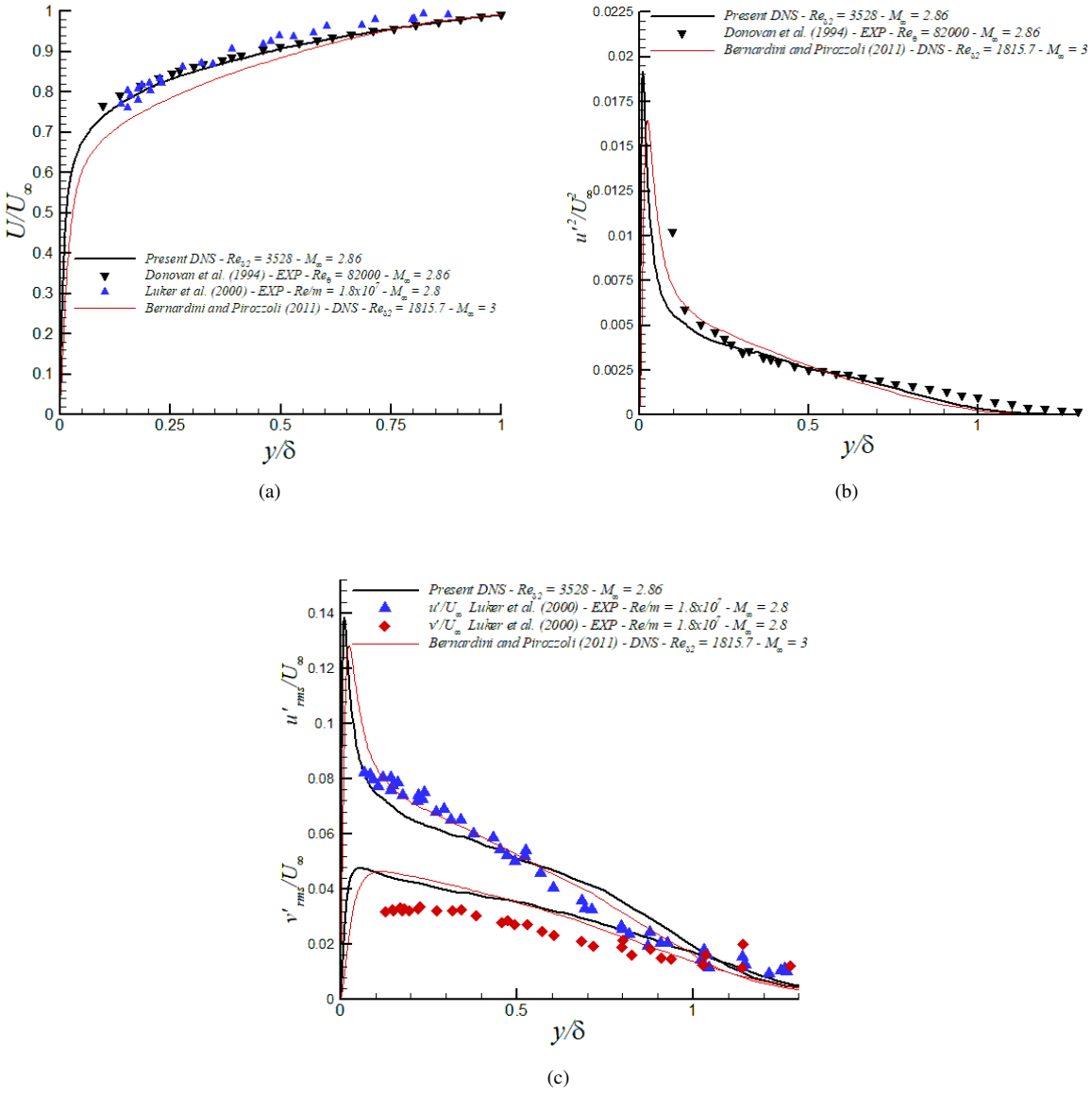

Fig. 4 (a) Mean streamwise velocity in outer units, (b) streamwise component of normal Reynolds stresses, and (c) turbulence intensities.

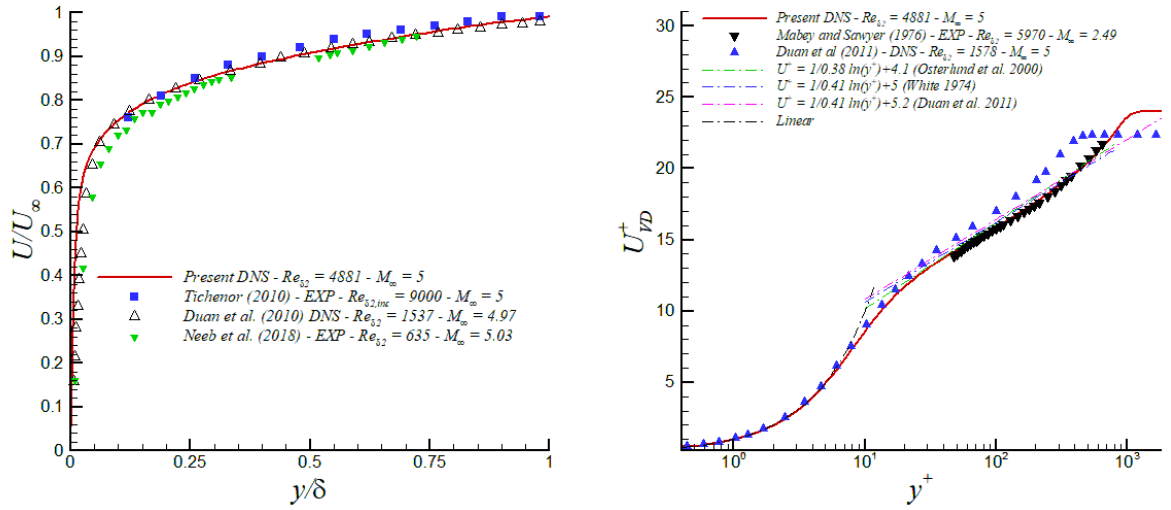

(a) (b)

Fig. 5 (a) Mean streamwise velocity in outer units, (b) mean streamwise velocity in inner units and the van Driest transformation.

B. High-Performance, FFT-based Energy Spectra Calculations

The energy spectra presented in this work were calculated leveraging the Python implementation of our in-house, out-of-core distributed library Aquila [6]. Aquila operates on larger-than-memory datasets efficiently via a high-performance data pre-fetcher capable of providing the illusion of an in-memory dataset. This is crucial given the limited amount of memory in modern supercomputing node architectures. The most recent implementation of Aquila leverages NumPy [48], SciPy [49], TBB [50, 51], Numba [52], MPI [53–56] and FFTW [57–63] to express the computations asynchronously and allowing for maximal parallelism with automatic out-of-core pre-fetch via a TBB-backed thread pool. To avoid over replication of arrays, Aquila instantiates one MPI rank per socket if sufficient RAM is available (one if the node is memory limited). Each rank coordinates a TBB thread pool assigning two threads per CPU core (i.e., SMT is enabled). Furthermore, TBB does not incorporate a central dealer as is the case with many multithreading schedulers; TBB implements private double-ended queues per worker and a sophisticated work stealing mechanism [50]. This again, makes our implementation highly scalable (see fig. 6) and decentralized at each level. Given the application has access to a fixed thread pool of workers, we decompose operations when possible into multiple independent, asynchronous tasks which enables latency hiding, high memory bandwidth and reasonable core utilization even when operating on out-of-core data. This implementation of Aquila enables the utilization of fast Fourier transforms for the calculation of both two point correlations and energy spectra in Fourier space [7, 8, 64] via the Convolution Theorem which yields high quality results at the expense of memory and lower arithmetic intensity compared to a matrix multiply implementation. Nonetheless, the results are far superior in terms of quality. We present a preliminary scaling study conducted at the Narwhal supercomputer out to 100 nodes with dual AMD Epyc Rome 7H12 CPUs. The nodes are interconnected with the HPE Cray Slingshot network at 200 Gb/s.

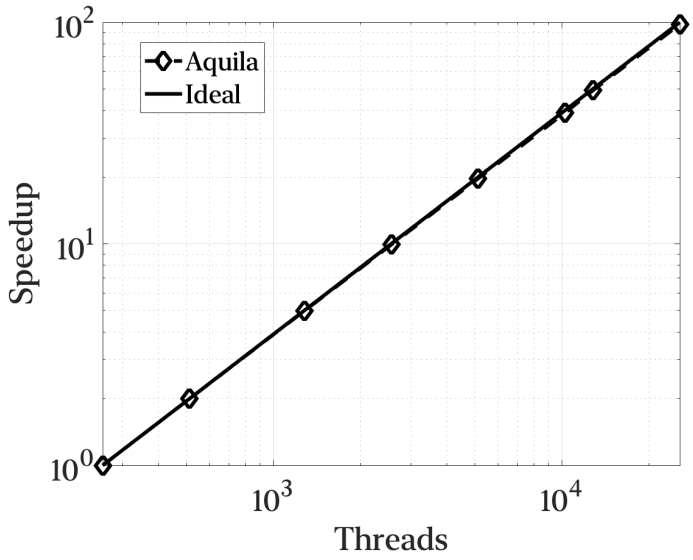

Fig. 6 Preliminary strong scaling analysis for Aquila conducted at the Narwhal supercomputer for the incompressible case presented in the present work.

V. Results and Discussion

A. Compressibility Effects on 1D Spectra

From figures 7, 8 and 9, we note that the compressibility effects on the normalized energy spectra are weak. This being said, the compressibility effects are more notable closer to the wall and in the streamwise spectra. A slight peak is observed and grows proportional to Mach number in the near-wall region. Furthermore, there appears to be a general trend in the reduction of the inertial subrange's thickness as Mach number increases. To more accurately assess the compressibility effects on the energy spectra, the spectra is multiplied by the wavenumber to highlight the energy content by unit length. This is often employed to filter the spectrum and it enables the identification of interesting energy concentrations at specific wavelengths. The pre-multiplied spectra is the focus of section V.B. The adequacy of

the mesh's resolution at the three flow conditions is reinforced by the slight energy buildup in the viscous dissipative subrange.

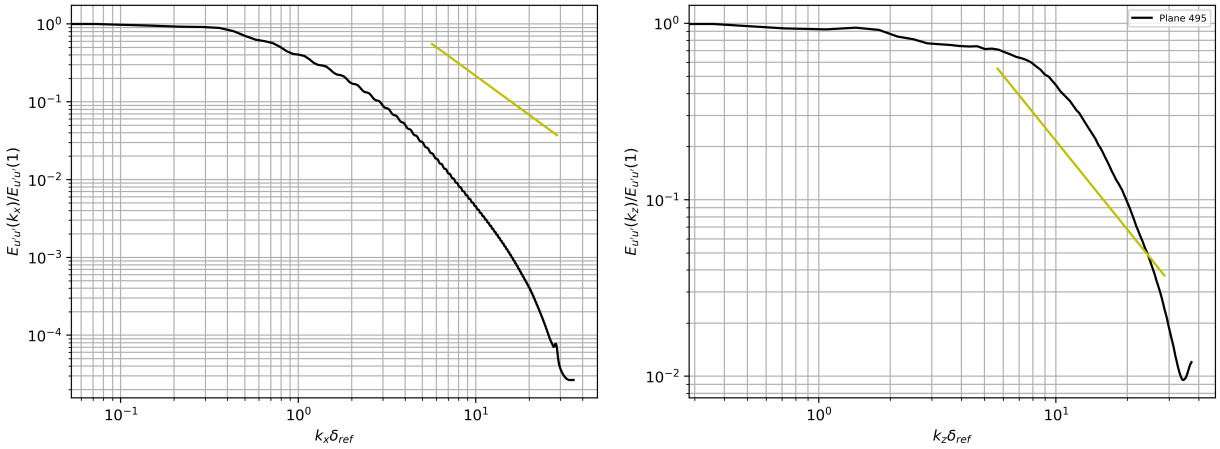

(a) Streamwise - Incompressible

(b) Spanwise - Incompressible

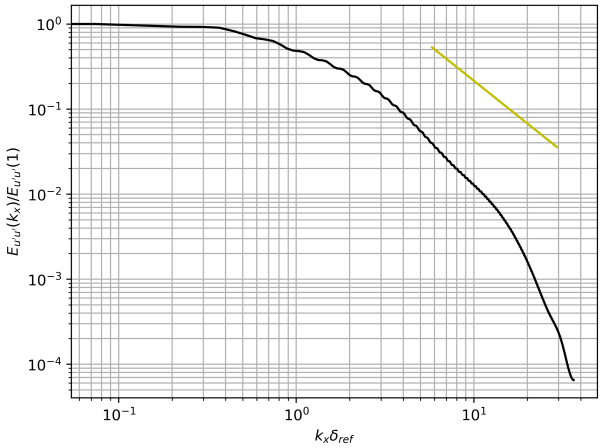

(c) Streamwise - $M_\infty = 2.86$

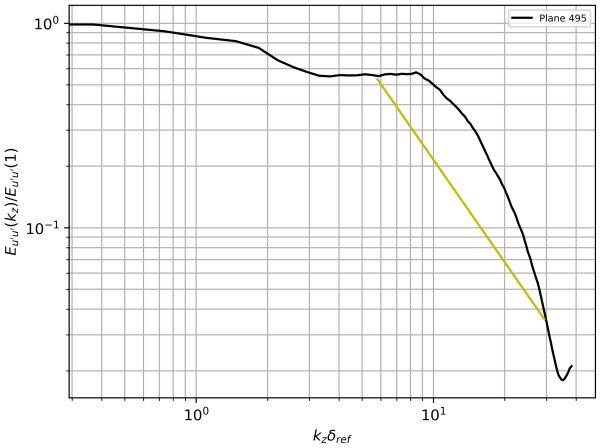

(d) Spanwise - $M_\infty = 2.86$

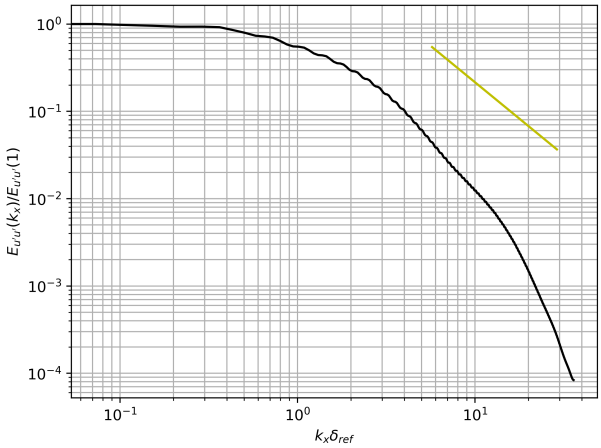

(e) Streamwise - $M_\infty = 5$

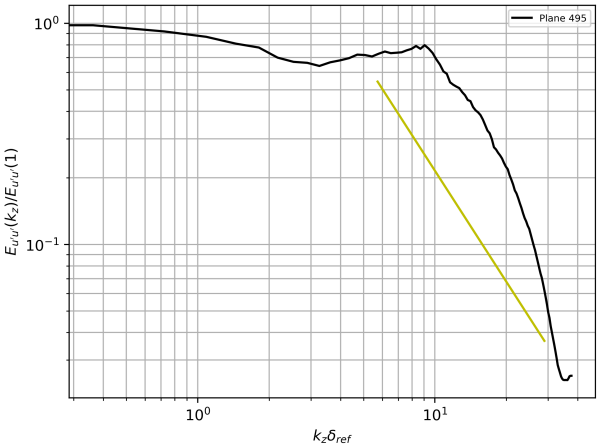

(f) Spanwise - $M_\infty = 5$

Fig. 7 Normalized streamwise $E_{u'u'}$ at $y^+ = 1$; the dashed line (- -) corresponds to a power law with exponent $-5/3$

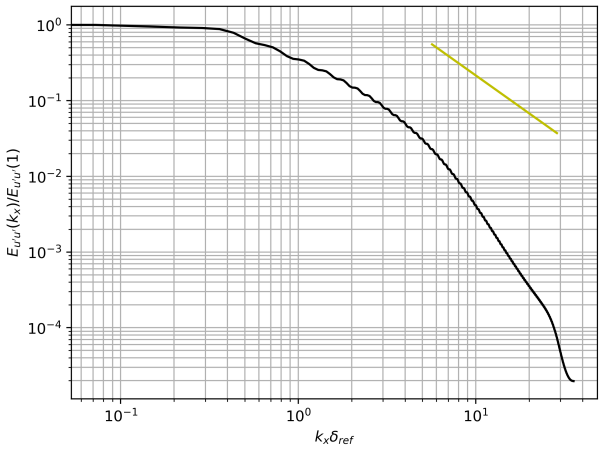

(a) Streamwise - Incompressible

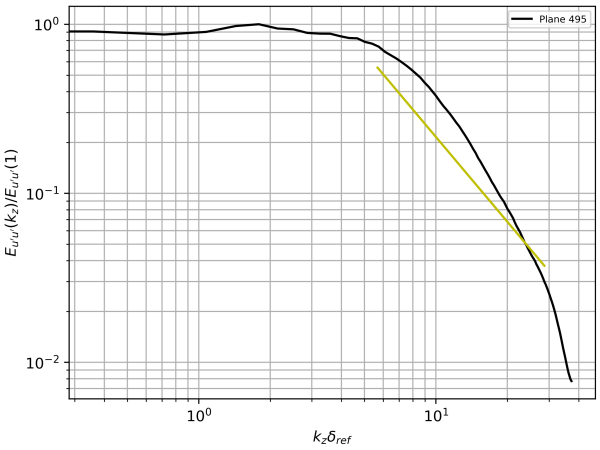

(b) Spanwise - Incompressible

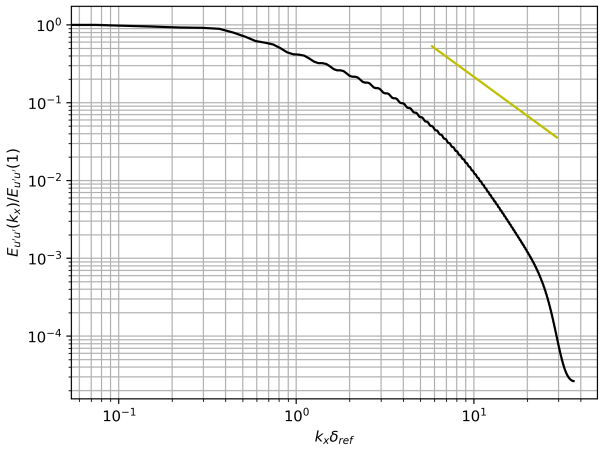

(c) Streamwise - $M_\infty = 2.86$

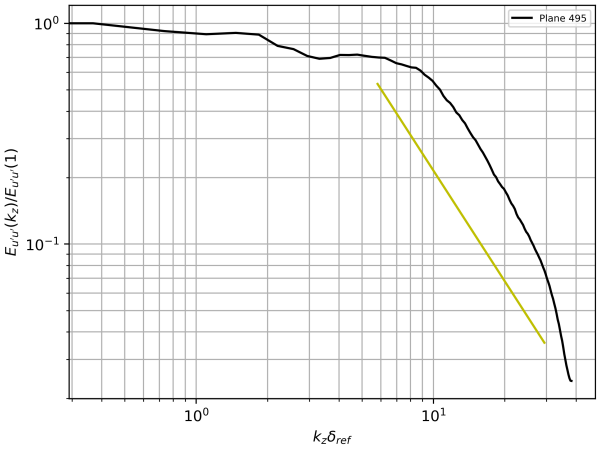

(d) Spanwise - $M_\infty = 2.86$

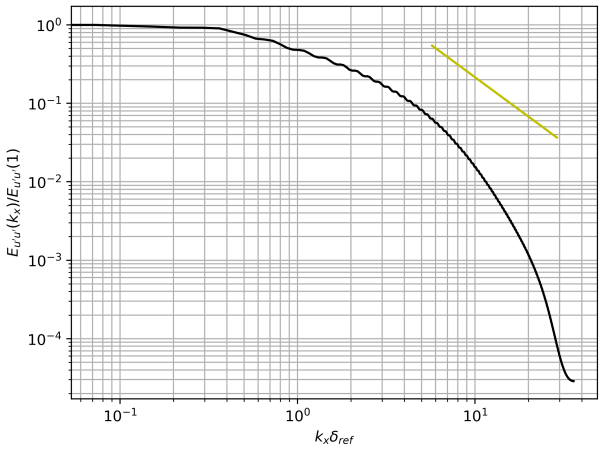

(e) Streamwise - $M_\infty = 5$

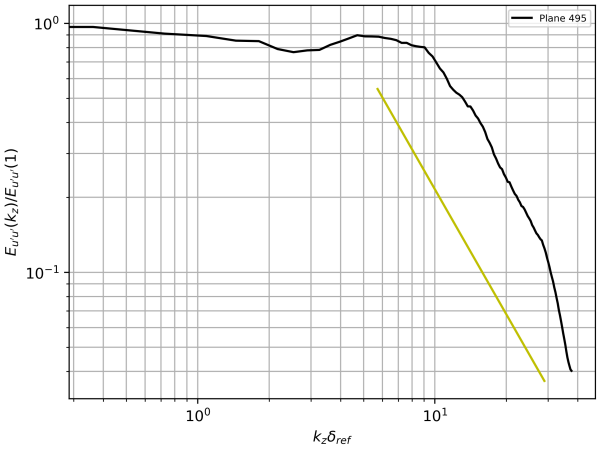

(f) Spanwise - $M_\infty = 5$

Fig. 8 Normalized $E_{u'u'}$ at $y^+ = 15$; the dashed line (- -) corresponds to a power law with exponent $-5/3$

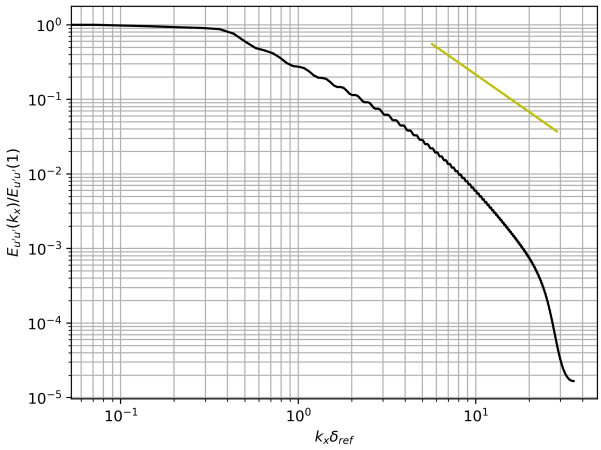

(a) Streamwise - Incompressible

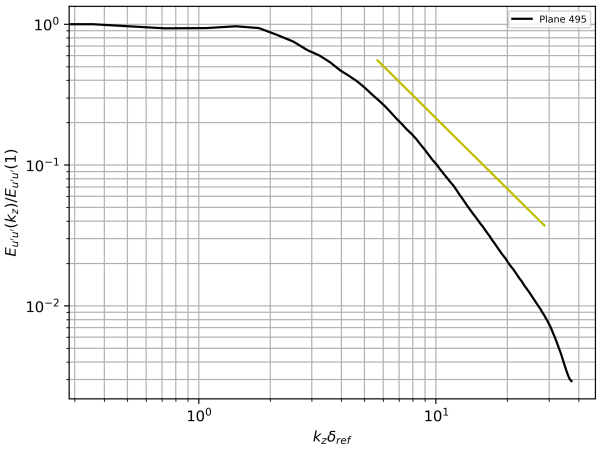

(b) Spanwise - Incompressible

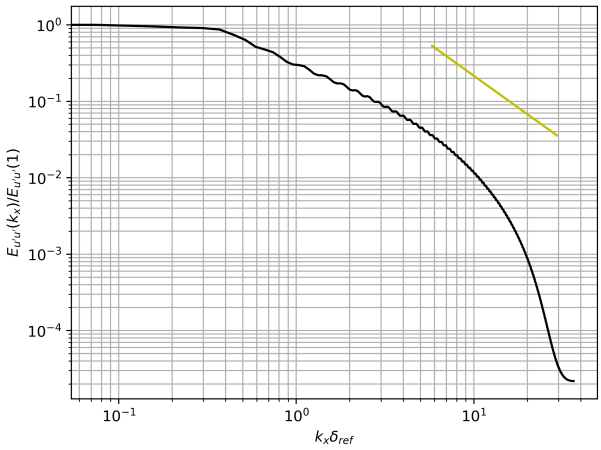

(c) Streamwise - $M_\infty = 2.86$

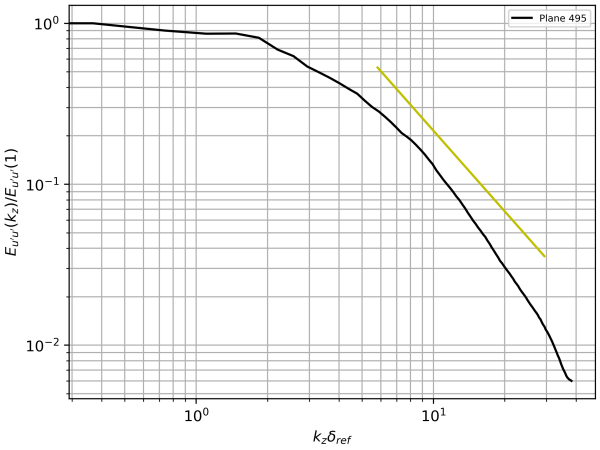

(d) Spanwise - $M_\infty = 2.86$

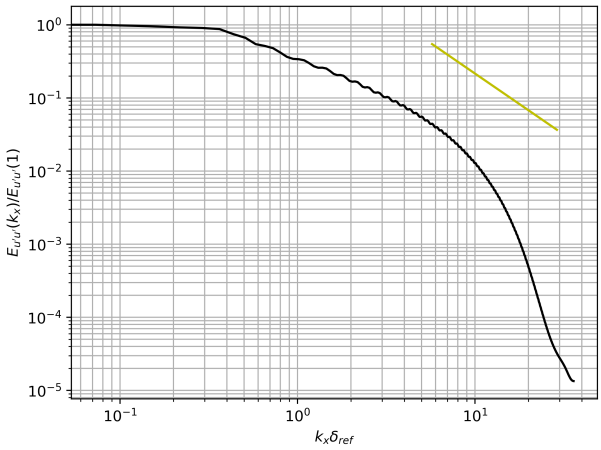

(e) Streamwise - $M_\infty = 5$

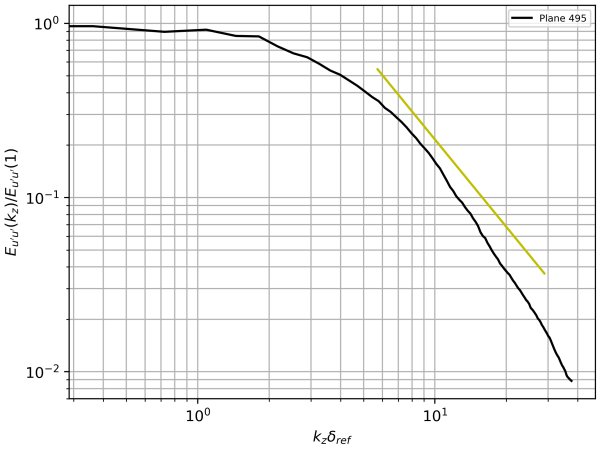

(f) Spanwise - $M_\infty = 5$

Fig. 9 Normalized $E_{u'u'}$ at $y^+ = 50$; the dashed line (- -) corresponds to a power law with exponent $-5/3$

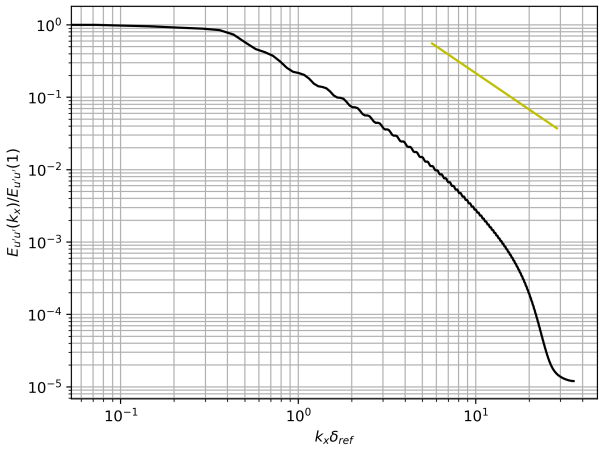

(a) Streamwise - Incompressible

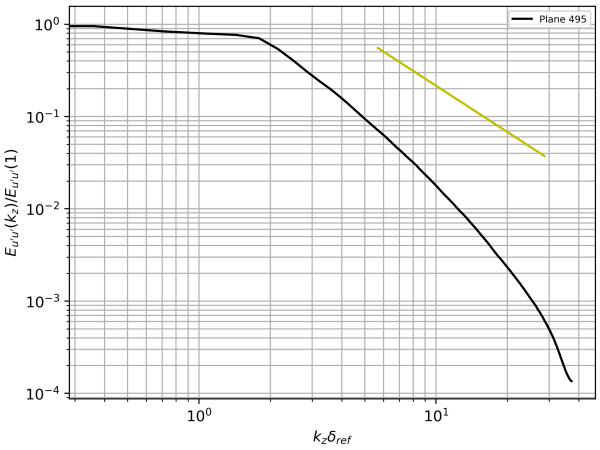

(b) Spanwise - Incompressible

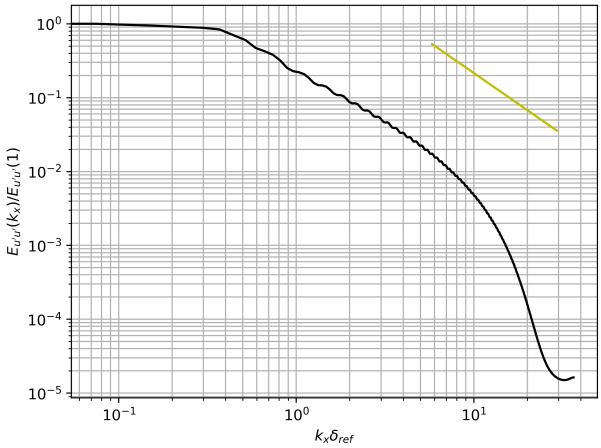

(c) Streamwise - $M_\infty = 2.86$

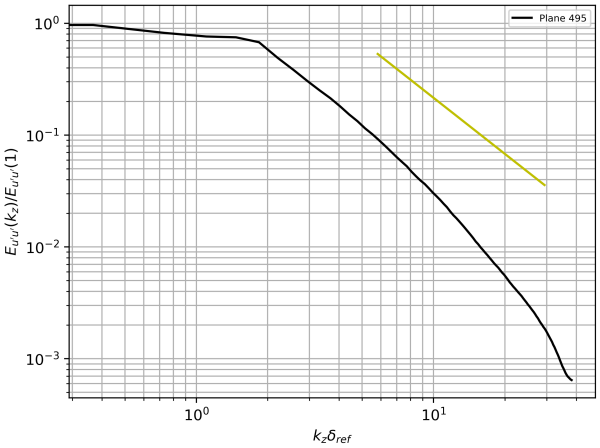

(d) Spanwise - $M_\infty = 2.86$

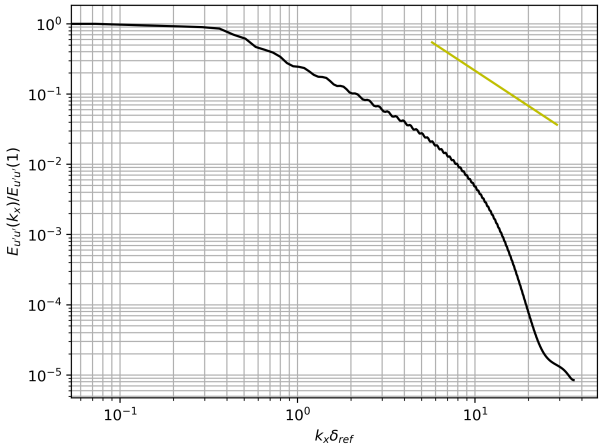

(e) Streamwise - $M_\infty = 5$

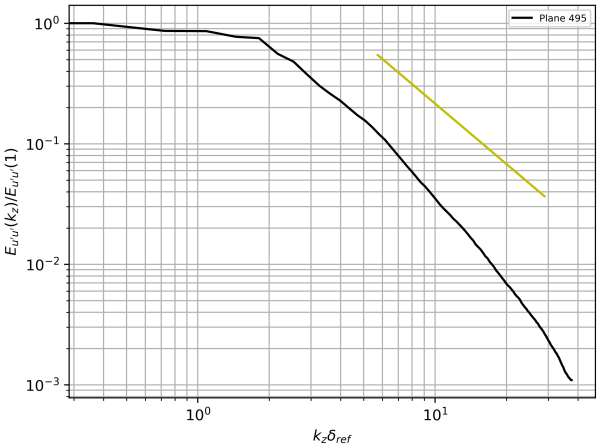

(f) Spanwise - $M_\infty = 5$

Fig. 10 Normalized $E_{u'u'}$ at $y^+ = 150$; the dashed line (- -) corresponds to a power law with exponent $-5/3$

B. Coherent Structure Characterization

Turbulent coherent structures and its wavelengths can be identified by visualizing the pre-multiplied spectra. Figures 11, 12 and 13 show the pre-multiplied energy spectra along the streamwise (a) and spanwise (b) as well as the streamwise component of the Reynolds normal stresses $(u'u')^+$ (c) in inner units at incompressible conditions and at Mach numbers of 2.86 and 5, respectively. In each set of images, the top two figures can be used to assess the streamwise and spanwise wavelengths of the dominant coherent structures at the different boundary layer regions. It is worth highlighting that the pre-multiplied spectra over u' has been performed without considering any density weighted time/space averaging in the present study. At all flow regimes, primary energy peaks are evident in the buffer region around $12 < y^+ < 15$, which are associated with spanwise wavelengths of the order of 100 wall units (or 0.1δ) and streamwise wavelengths of the order of 500 to 1000 wall units (much longer for the incompressible regime). This inner peak $\lambda_x^+ \approx$ 500-1000 (or 0.6 to 1 δ) is the energetic signature due to the viscous-scaled near-wall structure of elongated high- and low-speed regions, according to Hutchins and Marusic [4].

Additionally, one can see a weak (but still evident) secondary peak at spanwise wavelengths of the order of $\lambda_z^+ \approx 700$ (or 0.8δ) and streamwise wavelengths with $\lambda_x^+ \approx 3000$ (or 3δ's). These outer peaks of energy are somehow "hidden" by a strong energy "vestige" because of the near-wall structure ($\lambda_x^+ \approx$ 500-1000) and the moderate Reynolds numbers considered here, as well. The peak of $(u'u')^+$ occurs at approximately $y^+ = 15$ and a secondary peak can be detected for the incompressible and compressible (supersonic and hypersonic) cases at roughly $y^+ = 100 - 150$. This secondary peak is less obvious at the hypersonic regime. The coherent structures have a streamwise length of approximately 1δ, 0.7δ and 0.6δ for the incompressible, supersonic and hypersonic case at $y^+ = 15$. As expected, the turbulent structures associated with streamwise velocity fluctuations are significantly longer in the streamwise direction, showing an oblong shape. Interestingly, our pre-multiplied power spectra of u' along the spanwise direction for the supersonic case (fig. 12 (b)) exhibits a strong consistency with numerical results from Bernardini and Pirozzoli [38] (see their fig. 2b). They also performed DNS os a spatially-developing turbulent boundary layer at the supersonic regime (Mach 2) and with a friction Reynolds number of $Re_\tau = 1116$ (also known as δ^+), being our local $\delta^+ = 909$. It was also reported in [38] a secondary peak located at $y^+ \approx 180$ (and associated with spanwise wavelengths of $\lambda_z \approx 0.8\delta$) in agreement with the predicted locations of outer peaks by [65], i.e. $y^+ = 3.9\sqrt{Re_\tau}$. According to [38], the outer secondary peaks are the manifestation of the large scale motions in the logarithmic region of the boundary layer, whose signature on the inner region is noticeable under the form of low wavenumber energy "drainage" towards the wall.

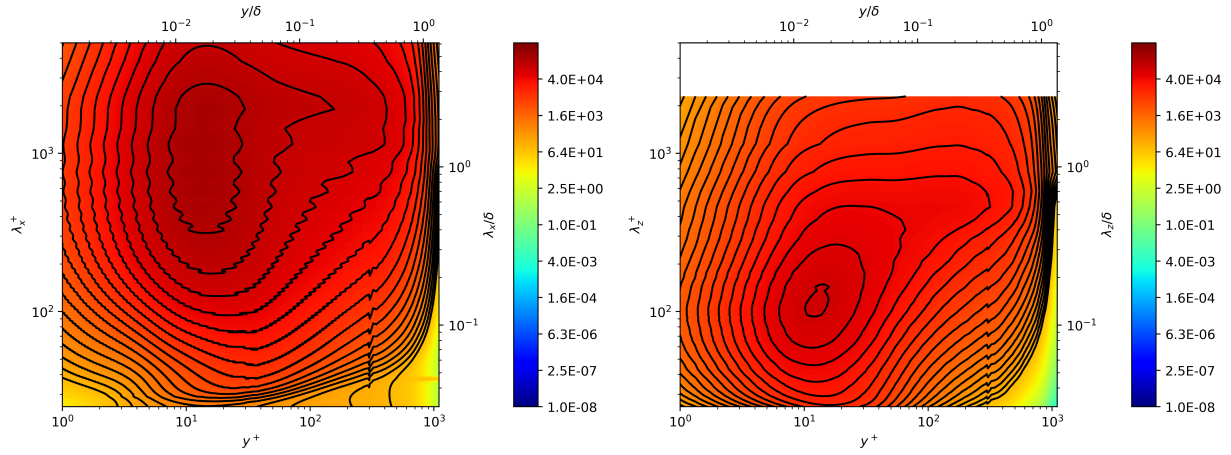

(a) Streamwise

(b) Spanwise

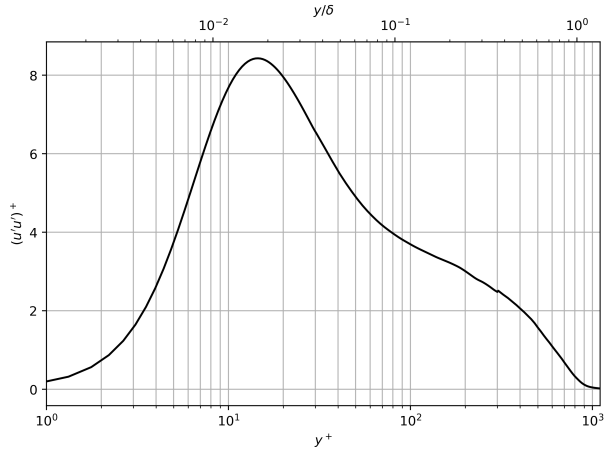

(c) $(u'u')^+$

Fig. 11 (a-b) Normalized, pre-multiplied spectra, $kE_{u'u'}/u_\tau^2$, at incompressible flow conditions; (c) Streamwise component of the Reynolds normal stresses

One notable finding in both figures 12b and 13b is a significant spanwise narrowing of the structures for the supersonic and hypersonic cases. A general trend shows a reduction in the dimensions as the Mach number grows as an evident compressibility effect. This can be confirmed by visualizing two point correlations in figures 14 in the buffer region at $y^+ = 15$. Furthermore, figure 14 suggests the range of influence of the coherent structure extends significantly along the downstream direction for the incompressible case ($\sim 1\delta$) and the shortening of the structures is mostly a diminution of its downstream influence (or tails). The length from the point of reference upstream is mostly unchanged from the incompressible to hypersonic (the change is $< 0.1\delta$) when compared to the downstream diminution ($\approx 0.35\delta$).

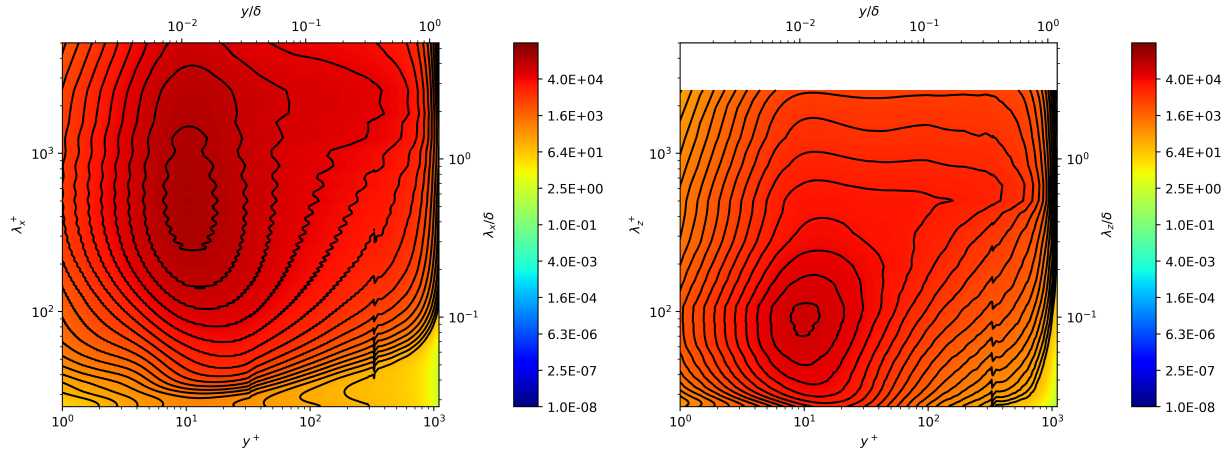

(a) Streamwise

(b) Spanwise

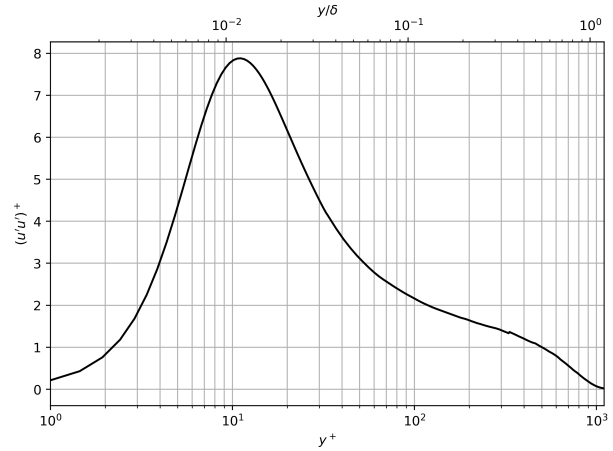

(c) $(u'u')^+$

Fig. 12 (a-b) Normalized, pre-multiplied spectra, $kE_{u'u'}/u_\tau^2$, at Mach 2.86; (c) Streamwise component of the Reynolds normal stresses.

This being said, the streamwise and spanwise dimensions of turbulent coherent structures via two-point correlations (TPC) in figure 14 are slightly consistent with the corresponding streamwise and spanwise wavelengths obtained in the pre-multiplied power spectra analysis, i.e. $\lambda_x \approx 0.6\text{-}1\delta$ and $\lambda_z \approx 0.1\delta$. The locations and magnitudes predicted from figures 11, 12 and 13 coincide with those reported in by Hutchins and Marusic [4] and in Bernardini and Pirozzoli [38].

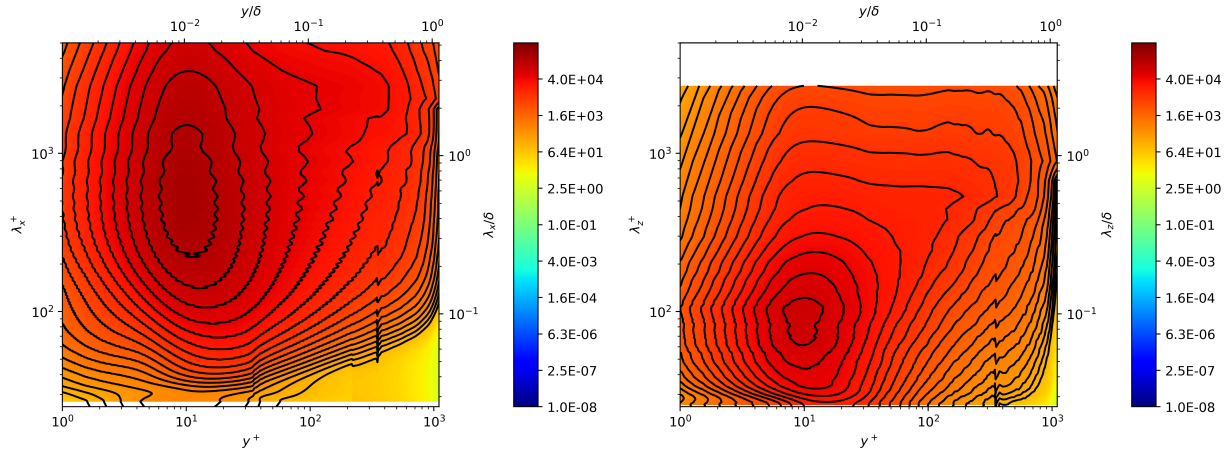

(a) Streamwise

(b) Spanwise

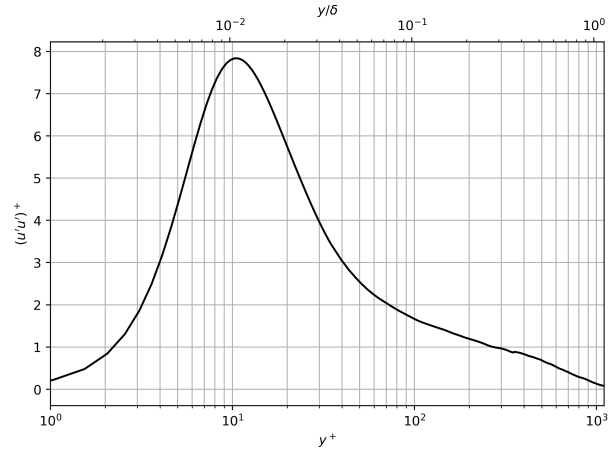

(c) $(u'u')^+$

Fig. 13 (a-b) Normalized, pre-multiplied spectra, $kE_{u'u'}/u_\tau^2$, at Mach 5; (c) Streamwise component of the Reynolds normal stresses.

As we previously mentioned, we present two point correlations near the peak of $(u'u')^+$ inside the boundary layer in figure 14. We computed the two point correlation via the convolution theorem which yields high resolution surfaces at low thresholds thus capturing more of the coherent structure without introducing spurious artifacts. In general, we observe a reduction in the size of the coherent structures as the Mach number increases.

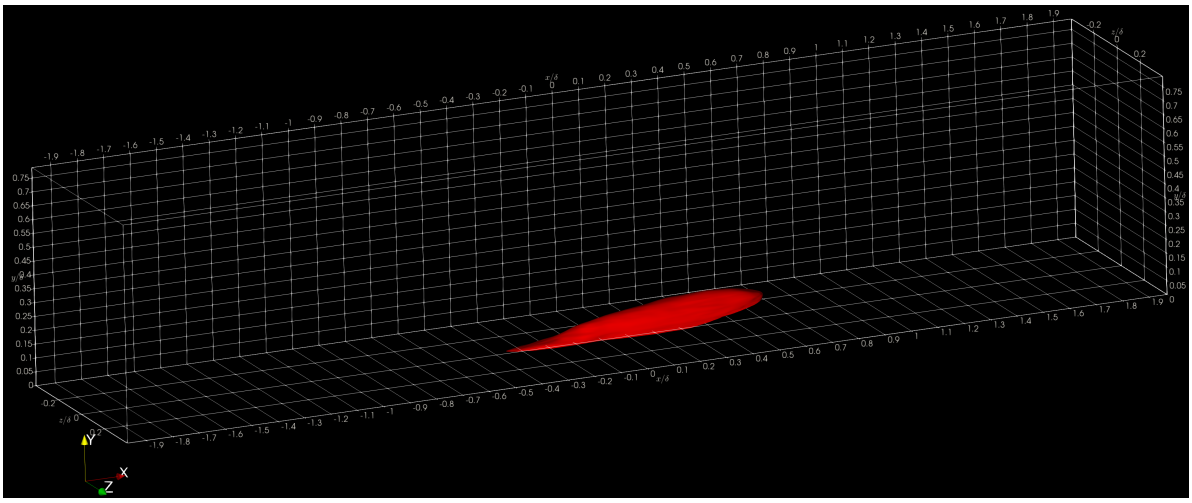

(a) Incompressible

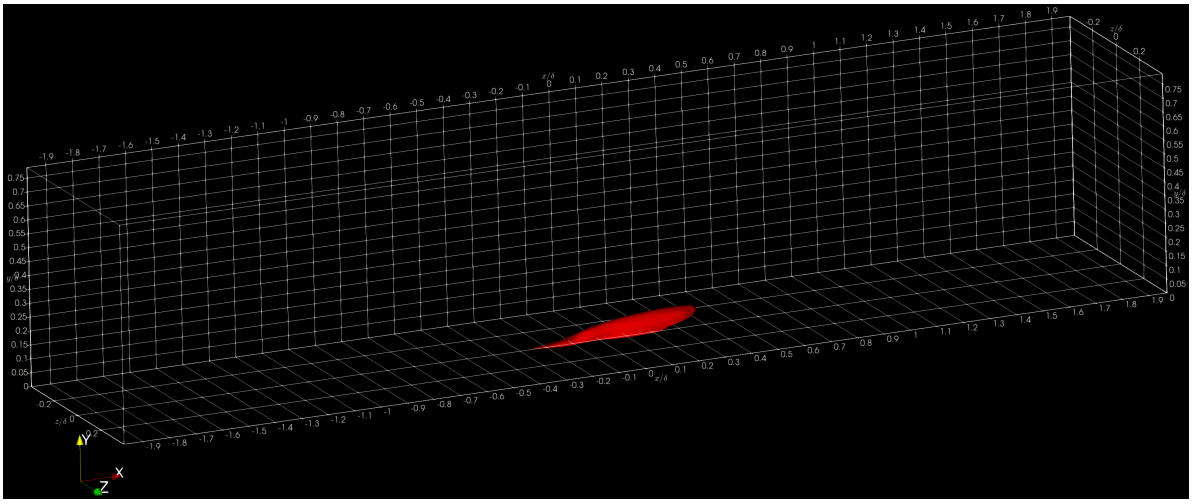

(b) Mach 2.86

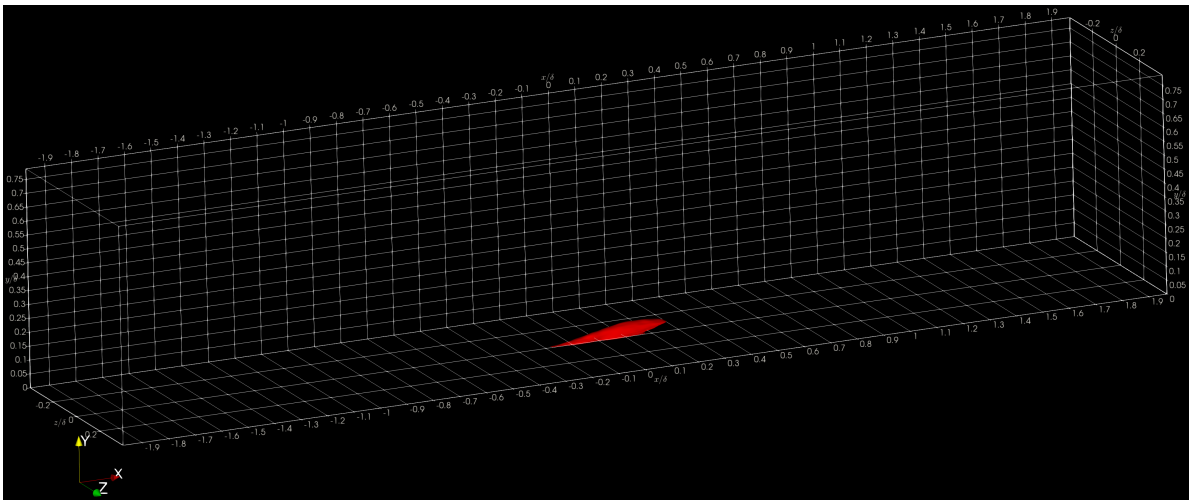

(c) Mach 5

Fig. 14 Two point correlations at $y^+ = 15$ at (a) incompressible, (b) Mach 2.86 and (c) Mach 5.

C. Inflow Quality Assessment

To assess the quality of the inflow condition generation method proposed by Araya *et al.* [1, 2], we visualize the energy spectra at multiple streamwise locations including the inlet and outlet planes to compare the structure of the energy spectra. The inflow plane's spectra is essentially indistinguishable from the middle plane in the near-wall region. In the outer region, the spectra is closer to that of the developed flow after 50 planes or roughly 1-δ.

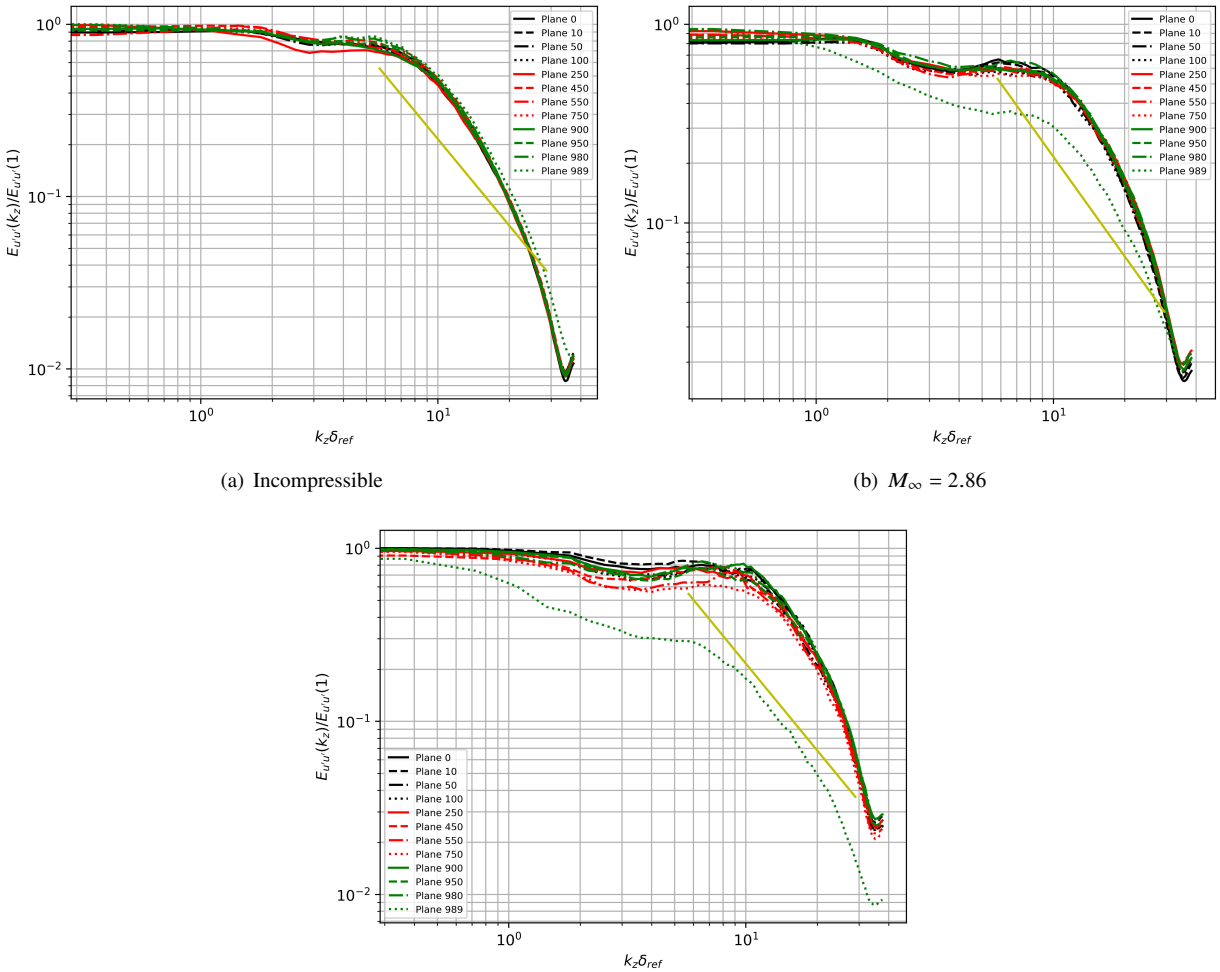

(a) Incompressible

(b) $M_\infty = 2.86$

(c) $M_\infty = 5$

Fig. 15 Normalized spanwise $E_{u'u'}$ at $y^+ = 1$ at multiple planes along the streamwise direction; the dashed line (- -) corresponds to a power law with exponent $-5/3$

What's more, the sponge outflow condition employed for the hypersonic case has a far more detrimental impact to the nature of the energy spectra in the near wall region than the inflow condition generated by the dynamic multiscale method as clearly seen from figures 15c and 16c. This is ameliorated as we probe farther from the wall as seen in fig. 17c.

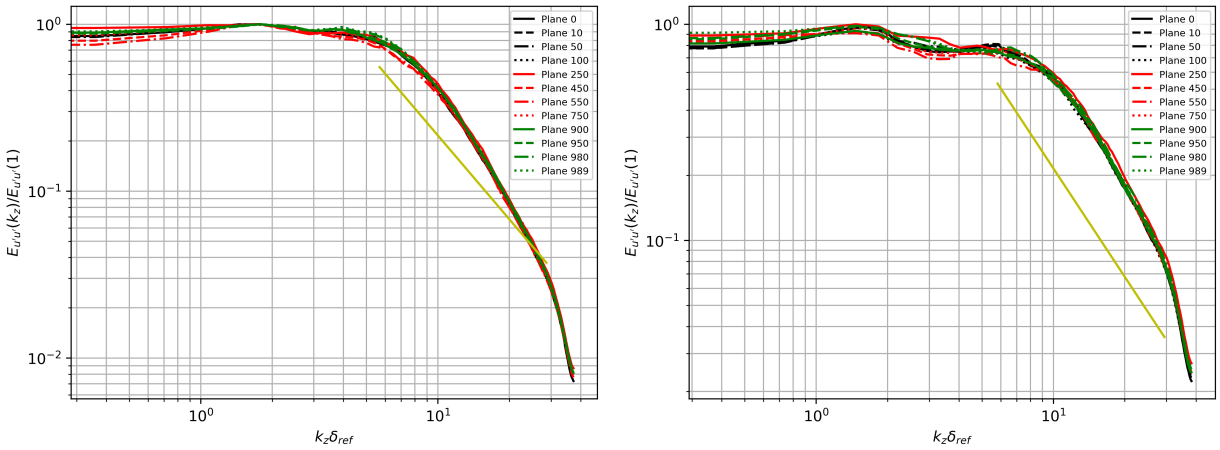

(a) Incompressible

(b) $M_\infty = 2.86$

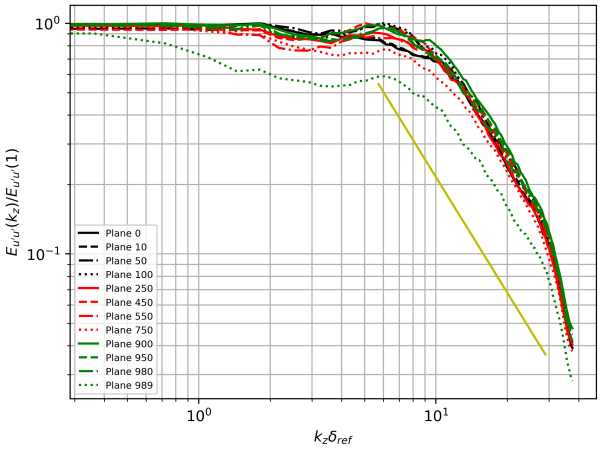

(c) $M_\infty = 5$

Fig. 16 Normalized spanwise $E_{u'u'}$ at $y^+ = 15$ at multiple planes along the streamwise direction; the dashed line (- -) corresponds to a power law with exponent $-5/3$

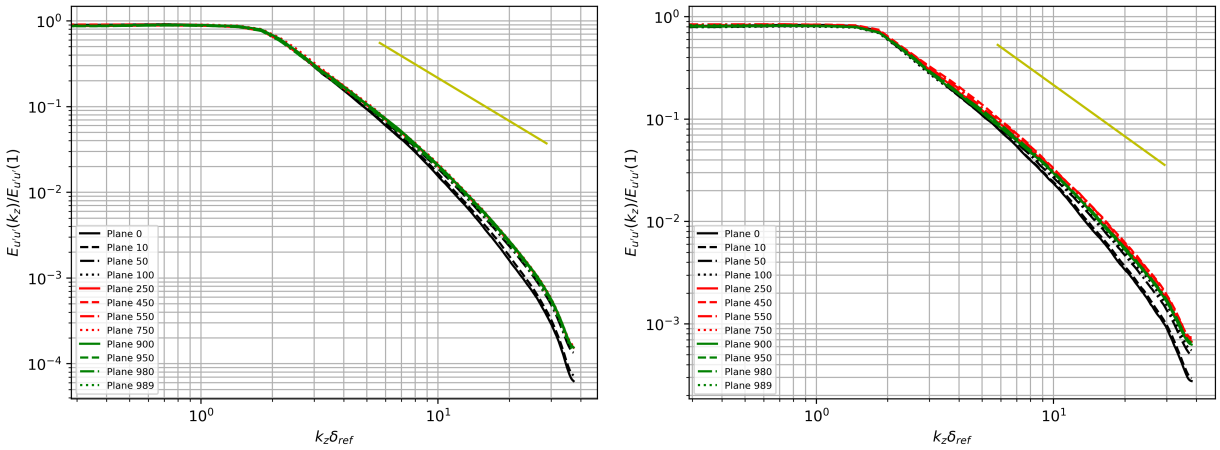

(a) Incompressible

(b) $M_\infty = 2.86$

(c) $M_\infty = 5$

Fig. 17 Normalized spanwise $E_{u'u'}$ at $y^+ = 150$ at multiple planes along the streamwise direction; the dashed line (- -) corresponds to a power law with exponent $-5/3$

VI. Future Work

We have computed additional spectra for $\overline{v'^2}$, $\overline{w'^2}$, $\overline{t'^2}$ and $\overline{p'^2}$, but we have not presented them in the interest of conciseness. Nonetheless, we plan to explore this additional correlations and incorporate cospectra to our future studies. Also, we plan to explore the potential of coherent structure identification based on wall thermal conditions.

VII. Conclusion

In this work, we performed a power spectra analysis to identify compressibility effects in the energy spectrum and assess the potential of coherent structure characterization via energy spectra analysis. The energy spectra were computed in the frequency domain employing a high-performance in house library for out-of-core computation. We compared three DNS cases at incompressible, Mach 2.86 and Mach 5 conditions. The compressibility effects in the normalized spectra are very weak. Nonetheless, they are more notable closer to the near wall region. Also, a reduction in the thickness of the inertial subrange (characterized as the region that follows the $-5/3$ slope) is seen as Mach number increases. In general, we observe a reduction in the dimensions of the coherent structures as Mach number increases. Further, as the Mach number grows, the structures become narrower and their downstream influence is notably diminished. The peak of $(u'u')^+$ coincides with the major peak in the pre-multiplied spectra at roughly $y^+ = 10 - 15$. Furthermore, we found an evident secondary peak at spanwise wavelengths of the order of $\lambda_z^+ \approx 700$ (or 0.8δ) and

streamwise wavelengths with $\lambda_x^+ \approx 3000$ (or 3δ's), which is in agreement with previous studies [4] [38]. We compared the dimensions predicted by pre-multiplied energy spectra analysis with those obtained via full domain 3D two-point correlations and found a strong agreement in the general trend. Additionally, the proposed inflow condition generation method proposed by Araya *et al.* [1, 2] was demonstrated to be highly robust with a minimal development region and an energy spectra resembling that of a fully developed flow. Interestingly, the outflow condition selection was found to have a more detrimental impact on the quality of the energy spectra at that plane.

Acknowledgments

This material is based upon work supported by the National Science Foundation under Grant No. HRD-1906130 and Grant No. 1847241. This work was supported in part by a grant from the Air Force Office of Scientific Research (grant no. FA9550-17-1-0051). This work was supported in part by a grant from the DoD High-Performance Computing Modernization Program (HPCMP).

References

[1] Araya, G., Castillo, L., Meneveau, C., and Jansen, K., " A dynamic multi-scale approach for turbulent inflow boundary conditions in spatially evolving flows," *Journal of Fluid Mechanics*, Vol. 670, 2011, pp. 518–605.

[2] Araya, G., Lagares, C., and Jansen, K., "Reynolds number dependency in supersonic spatially-developing turbulent boundary layers," *2020 AIAA SciTech Forum (AIAA 3247313) 6 - 10 January, Orlando, FL.*, 2020.

[3] Jimenéz, J., "Coherent structures in wall-bounded turbulence," *Journal of Fluid Mechanics*, Vol. 842, 2018, p. 842.

[4] Hutchins, N., and Marusic, I., "Large-scale influences in near-wall turbulence," *Phil. Trans. R. Soc.*, Vol. 365, 2007, pp. 647–664.

[5] Pope, S. B., *Turbulent Flows*, Cambridge University Press, 2000.

[6] C. J. Lagares, Rivera, W., and Araya, G., "Aquila: A Distributed and Portable Post-Processing Library for Large-Scale Computational Fluid Dynamics," *AIAA SciTech*, 2021.

[7] Arfken, G., *Mathematical Methods for Physicists*, Academic Press, 1985.

[8] Bracewell, R., *The Fourier Transform and Its Applications*, New York: McGraw-Hill, 1999.

[9] Spina, E. F., and Smits, A. J., "Organized structures in a compressible, turbulent boundary layer," *Journal of Fluid Mechanics*, Vol. 182, 1987, pp. 85–109.

[10] Rempfer, D., and Fasel, H. F., "Dynamics of three-dimensional coherent structures in a flat-plate boundary layer," *Journal of Fluid Mechanics*, Vol. 275, 1994, pp. 257–283.

[11] Aubry, N., Holmes, P., Lumley, J. L., and Stone, E., "The dynamics of coherent structures in the wall region of a turbulent boundary layer," *Journal of Fluid Mechanics*, Vol. 192, 1988, pp. 115–173.

[12] Smits, A. J., Spina, E. F., Alving, A. E., Smith, R. W., Fernando, E. M., and Donovan, J. F., "A comparison of the turbulence structure of subsonic and supersonic boundary layers," *Physics of Fluids*, Vol. 1, No. 11, 1989, pp. 1865–1875.

[13] Ringuette, M. J., Wu, M., and Martin, M. P., "Coherent structures in direct numerical simulation of turbulent boundary layers at Mach 3," *Journal of Fluid Mechanics*, Vol. 594, 2008, pp. 59–69.

[14] Elsinga, G. E., Adrian, R. J., van Oudheusden, B. W., and Scarano, F., "Three-dimensional vortex organization in a high-Reynolds-number supersonic turbulent boundary layer," *Journal of Fluid Mechanics*, Vol. 644, 2010, pp. 35–60.

[15] Lin, H., ShiHe, Y., YuXin, Z., LiFeng, T., and Zhi, C., "Visualization of Coherent Structures in a Supersonic Flat-Plate Boundary Layer," *Chinese Science Bulletin*, Vol. 56, No. 6, 2011, pp. 489–494.

[16] Sillero, J., Jimenez, J., and Moser, R., "Two-point statistics for turbulent boundary layers and channels at Reynolds numbers up to $\delta^+ \approx 2000$," *Physics of Fluids*, Vol. 26, No. 10, 2014, 105109.

[17] Dharmarathne, S., Tutkun, M., Araya, G., and Castillo, L., "Structures of scalar transport in a turbulent channel," *European Journal of Mechanics B-Fluids*, Vol. 55, No. 2, 2016, pp. 259–271.

[18] Araya, G., C. J. Lagares, Santiago, J., and Jansen, K., "Wall temperature effect on hypersonic turbulent boundary layers via DNS," *AIAA SciTech*, 2021.

[19] Hutchins, N., and Marusic, I., "Evidence of very long meandering features in the logarithmic region of turbulent boundary layers," *Journal of Fluid Mechanics*, Vol. 579, 2007, pp. 1–28.

[20] "Scaling of the energy spectra of turbulent channels," *Journal of Fluid Mechanics*, Vol. 500, 2004, pp. 135–144. https://doi.org/10.1017/S002211200300733X.

[21] Sharp, N. S., Neuscamman, S., and Warhaft, Z., "Effects of large-scale free stream turbulence on a turbulent boundary layer," Vol. Physics of Fluids, 2009. https://doi.org/10.1063/1.3225146.

[22] Huang, J., Zhang, C., Duan, L., and Choudhari, M. M., "Direct numerical simulation of hypersonic turbulent boundary layers inside an axisymmetric nozzle," *55th AIAA Aerospace Sciences Meeting*, 2017, p. 0067.

[23] Martin, M. P., "Direct numerical simulation of hypersonic turbulent boundary layers. Part 1. Initialization and comparison with experiments," *Journal of Fluid Mechanics*, Vol. 570, 2007, pp. 347–364.

[24] Jansen, K., "Unstructured grid large eddy simulation of wall bounded flow," *Annual Research Briefs*, Center for Turbulence Research, NASA Ames / Stanford University, 1993, pp. 151–156.

[25] Jansen, K. E., "A stabilized finite element method for computing turbulence," *Comp. Meth. Appl. Mech. Engng.*, Vol. 174, 1999, pp. 299–317.

[26] Jansen, K. E., Whiting, C. H., and Hulbert, G. M., "A generalized-α method for integrating the filtered Navier-Stokes equations with a stabilized finite element method," *Comp. Meth. Appl. Mech. Engng.*, Vol. 190, 1999, pp. 305–319.

[27] Whiting, C. H., Jansen, K. E., and Dey, S., "Hierarchical basis in stabilized finite element methods for compressible flows," *Comp. Meth. Appl. Mech. Engng.*, Vol. 192, No. 47-48, 2003, pp. 5167–5185.

[28] Araya, G., Lagares, C., and Jansen, K., "Direct simulation of a Mach-5 turbulent spatially-developing boundary layer," *49^{th} AIAA Fluid Dynamics Conference, AIAA AVIATION Forum, (AIAA 3131876) 17 - 21 June, Dallas, TX*, 2019.

[29] Lund, T., Wu, X., and Squires, K., "Generation of turbulent inflow data for spatially-developing boundary layer simulations," *Journal of Computational Physics*, Vol. 140, No. 2, 1998, pp. 233–258.

[30] G. Urbin and D. Knight, "Large-Eddy Simulation of a supersonic boundary layer using an unstructured grid," *AIAA Journal*, Vol. 39, No. 7, 2001, pp. 1288–1295.

[31] Stolz, S., and Adams, N., "Large-eddy simulation of high-Reynolds-number supersonic boundary layers using the approximate deconvolution model and a rescaling and recycling technique," *Physics of Fluids*, Vol. 15, No. 8, 2003, pp. 2398–2412.

[32] Xu, S., and Martin, M. P., "Assessment of inflow boundary conditions for compressible turbulent boundary layers," *Physics of Fluids*, Vol. 16, No. 7, 2004, pp. 2623–2639.

[33] Kistler, A., and Chen, W., "A Fluctuating Pressure Field in a Supersonic Turbulent Boundary Layer," *Journal of Fluid Mechanics*, Vol. 16, 1963, pp. 41–64.

[34] Araya, G., Castillo, C., and Hussain, F., "The log behaviour of the Reynolds shear stress in accelerating turbulent boundary layers," *Journal of Fluid Mechanics*, Vol. 775, 2015, pp. 189–200.

[35] Doosttalab, A., Araya, G., Newman, J., Adrian, R., Jansen, K., and Castillo, L., "Effect of small roughness elements on thermal statistics of a turbulent boundary layer at moderate Reynolds number," *Journal of Fluid Mechanics*, Vol. 787, 2015, pp. 84–115.

[36] Stalmach, C., "Experimental Investigation of the Surface Impact Pressure Probe Method Of Measuring Local Skin Friction at Supersonic Speeds," *Bureau of Engineering Research, University of Texas*, 1958.

[37] Pirozzoli, S., and Bernardini, M., "Turbulence in supersonic boundary layers at moderate Reynolds number," *Journal of Fluid Mechanics*, Vol. 688, 2011, pp. 120–168.

[38] Bernardini, M., and Pirozzoli, S., "Wall pressure fluctuations beneath supersonic turbulent boundary layers," *Phys. Fluids*, 2011, p. 085102.

[39] PIPONNIAU, S., DUSSAUGE, J., DEBIEVE, J. F., and DUPONT, P., "A simple model for low-frequency unsteadiness in shock-induced separation," *Journal of Fluid Mechanics*, Vol. 629, 2009, pp. 87–108.

[40] Donovan, J., Spina, E., and Smits, A., "The structure of a supersonic turbulent boundary layer subjected to concave surface curvature," *Journal of Fluid Mechanics*, Vol. 259, 1994, pp. 1–24.

[41] Luker, J. J., Bowersox, R. D. W., and Buter, T. A., "Influence of Curvature-Driven Favorable Pressure Gradient on Supersonic Turbulent Boundary Layer," *AIAA Journal*, Vol. 38, No. 8, 2000, pp. 1351–1359. https://doi.org/10.2514/2.1134.

[42] Tichenor, N. T., "Characterization of the influence of a favorable pressure gradient on the basic structure of a Mach 5.0 high Reynolds number supersonic turbulent boundary layer," *Ph.D. dissertation, Texas A and M University*, 2010.

[43] Duan, L. and Beekman, I. and Martin, M. P., "Direct numerical simulation of hypersonic turbulent boundary layers. Part 3. Effect of Mach number," *Journal of Fluid Mechanics*, Vol. 672, 2011, pp. 245–267.

[44] Neeb, D., Saile, D., and Gulhan, A., "Experiments on a smooth wall hypersonic boundary layer at Mach 6," *Experiments in Fluids*, Vol. 59 (68), 2018.

[45] D. Mabey and W. Sawyer, "Experimental Studies of the Boundary Layer on a Flat Plate at Mach Numbers from 2.5 to 4.5," *Aerodynamics Department, R.A.E., Bedford.*, Vol. Reports and Memoranda No. 3784, 1976.

[46] White, F. M., *Viscous Fluid Flow*, McGraw-Hill Mechanical Engineering, New York, 2006.

[47] Osterlund, J. M., Johansson, A. V., Nagib, H. M., and Hites, M. H., "A note on the overlap region in turbulent boundary layers," *Physics of Fluids*, Vol. 12, 2001.

[48] Harris, C. R., Millman, K. J., van der Walt, S. J., Gommers, R., Virtanen, P., Cournapeau, D., Wieser, E., Taylor, J., Berg, S., Smith, N. J., Kern, R., Picus, M., Hoyer, S., van Kerkwijk, M. H., Brett, M., Haldane, A., del Río, J. F., Wiebe, M., Peterson, P., Gérard-Marchant, P., Sheppard, K., Reddy, T., Weckesser, W., Abbasi, H., Gohlke, C., and Oliphant, T. E., "Array programming with NumPy," *Nature*, Vol. 585, No. 7825, 2020, pp. 357–362. https://doi.org/10.1038/s41586-020-2649-2, URL https://doi.org/10.1038/s41586-020-2649-2.

[49] Virtanen, P., Gommers, R., Oliphant, T. E., Haberland, M., Reddy, T., Cournapeau, D., Burovski, E., Peterson, P., Weckesser, W., Bright, J., van der Walt, S. J., Brett, M., Wilson, J., Millman, K. J., Mayorov, N., Nelson, A. R. J., Jones, E., Kern, R., Larson, E., Carey, C. J., Polat, İ., Feng, Y., Moore, E. W., VanderPlas, J., Laxalde, D., Perktold, J., Cimrman, R., Henriksen, I., Quintero, E. A., Harris, C. R., Archibald, A. M., Ribeiro, A. H., Pedregosa, F., van Mulbregt, P., and SciPy 1.0 Contributors, "SciPy 1.0: Fundamental Algorithms for Scientific Computing in Python," *Nature Methods*, Vol. 17, 2020, pp. 261–272. https://doi.org/10.1038/s41592-019-0686-2.

[50] Pheatt, C., "Intel® Threading Building Blocks," *J. Comput. Sci. Coll.*, Vol. 23, No. 4, 2008, p. 298.

[51] Anton Malakhov, David Liu, Anton Gorshkov, and Terry Wilmarth, "Composable Multi-Threading and Multi-Processing for Numeric Libraries," *Proceedings of the 17th Python in Science Conference*, edited by Fatih Akici, David Lippa, Dillon Niederhut, and M. Pacer, 2018, pp. 18 – 24. https://doi.org/10.25080/Majora-4af1f417-003.

[52] Lam, S. K., Pitrou, A., and Seibert, S., "Numba: A LLVM-Based Python JIT Compiler," *Proceedings of the Second Workshop on the LLVM Compiler Infrastructure in HPC*, Association for Computing Machinery, New York, NY, USA, 2015. https://doi.org/10.1145/2833157.2833162, URL https://doi.org/10.1145/2833157.2833162.

[53] "MPI: A message passing interface," *Supercomputing '93:Proceedings of the 1993 ACM/IEEE Conference on Supercomputing*, 1993, pp. 878–883. https://doi.org/10.1109/SUPERC.1993.1263546.

[54] Dalcín, L., Paz, R., and Storti, M., "MPI for Python," *Journal of Parallel and Distributed Computing*, Vol. 65, No. 9, 2005, pp. 1108–1115. https://doi.org/https://doi.org/10.1016/j.jpdc.2005.03.010, URL https://www.sciencedirect.com/science/article/pii/S0743731505000560.

[55] Dalcín, L., Paz, R., Storti, M., and D'Elía, J., "MPI for Python: Performance improvements and MPI-2 extensions," *Journal of Parallel and Distributed Computing*, Vol. 68, No. 5, 2008, pp. 655–662. https://doi.org/https://doi.org/10.1016/j.jpdc.2007.09.005, URL https://www.sciencedirect.com/science/article/pii/S0743731507001712.

[56] Dalcin, L. D., Paz, R. R., Kler, P. A., and Cosimo, A., "Parallel distributed computing using Python," *Advances in Water Resources*, Vol. 34, No. 9, 2011, pp. 1124–1139. https://doi.org/https://doi.org/10.1016/j.advwatres.2011.04.013, URL https://www.sciencedirect.com/science/article/pii/S0309170811000777, new Computational Methods and Software Tools.

[57] Frigo, M., and Johnson, S. G., "The Design and Implementation of FFTW3," *Proceedings of the IEEE*, Vol. 93, No. 2, 2005, pp. 216–231. Special issue on "Program Generation, Optimization, and Platform Adaptation".

[58] Johnson, S. G., and Frigo, M., "Implementing FFTs in Practice," *Fast Fourier Transforms*, edited by C. S. Burrus, Connexions, Rice University, Houston TX, 2008, Chap. 11. URL http://cnx.org/content/m16336/.

[59] Frigo, M., "A fast Fourier transform compiler," *Proc. 1999 ACM SIGPLAN Conf. on Programming Language Design and Implementation*, Vol. 34, ACM, 1999, pp. 169–180.

[60] Frigo, M., and Johnson, S. G., "FFTW: An adaptive software architecture for the FFT," *Proc. 1998 IEEE Intl. Conf. Acoustics Speech and Signal Processing*, Vol. 3, IEEE, 1998, pp. 1381–1384.

[61] Frigo, M., and Johnson, S. G., "The Fastest Fourier Transform in the West," Tech. Rep. MIT-LCS-TR-728, Massachusetts Institute of Technology, September 1997.

[62] Frigo, M., Leiserson, C. E., Prokop, H., and Ramachandran, S., "Cache-oblivious algorithms," *Proc. 40th Ann. Symp. on Foundations of Comp. Sci. (FOCS)*, IEEE Comput. Soc., 1999, pp. 285–297.

[63] Johnson, S. G., and Frigo, M., "A modified split-radix FFT with fewer arithmetic operations," *IEEE Trans. Signal Processing*, Vol. 55, No. 1, 2007, pp. 111–119.

[64] Box, G. E. P., Jenkins, G. M., Reinsel, G. C., and Ljung, G. M., *Time Series Analysis: Forecasting and Control*, 2015.

[65] Mathis, R., Hutchins, N., and Marusic, I., "Large-scale amplitude modulation of the small-scale structures in turbulent boundary layers," *J. Fluid Mech.*, Vol. 628, 2009, p. 311.